Quaternary International 695 (2024) 1–17

Contents lists available at ScienceDirect

Quaternary International

journal homepage: www.elsevier.com/locate/quaint

Late Quaternary transgressions and regressions in the Trieste Gulf (north-eastern Adriatic Sea)

Massimo Zecchin [a,*], Mauro Caffau [a], Martina Busetti [a], Carlo Alberto Masoli [b], Luca Baradello [a], Dario Civile [a], Michela Dal Cin [a], Lorenzo Petronio [a], Roberto Romeo [a], Luigi Sante Zampa [a], Davide Lenaz [c], Renata Giulia Lucchi [a], Andrea Caburlotto [a]

[a] National Institute of Oceanography and Applied Geophysics - OGS, 34010, Sgonico, TS, Italy
[b] Geosyntech s.r.l., Trieste, Italy
[c] Department of Mathematics, Informatics and Geosciences, University of Trieste, 34128, Trieste, Italy

ARTICLE INFO

Keywords:
Trieste gulf
Glacio-eustasy
Tyrrhenian
Transgressive-regressive sequences
Younger Dryas

ABSTRACT

The integration of high-resolution seismic profiles, core data and radiocarbon plus U-Th datings, allows to document the late Quaternary succession of the Trieste Gulf, which represents the easternmost part of the northern Adriatic Sea. This succession consists of an alternation of shallow-marine and continental deposits organized to compose four transgressive-regressive sequences down to ca. 90 m below present sea level. The sequences terminate landwards against a stepped surface bounding the Eocene Trieste Flysch and produced by alternating episodes of wave erosion during transgressions and subaerial exposure during stages of relative sea-level fall and lowstand. Two shallow-marine wedges, in addition to the Holocene one, have been recognized; they are associated with the Marine Isotopic Stage (MIS) 5.5 (Tyrrhenian) and probably at least one of the peaks of MIS 7. The recognized shallow-marine wedges typically prograde just seaward of a buried wave-cut platform lying in front of a receding paleo-coastal cliff. A previously unrecognized stratigraphic hiatus of ca. 25 ka duration, containing the whole Last Glacial Maximum (LGM) phase, was found at the top of palustrine deposits that accumulated on the MIS 5.5 marine sediments until ca. 40 cal ka B.P. and a post-LGM peat bed accumulated during the Younger Dryas stadial. The beginning of the Holocene was characterized by marked fluvial aggradation preceding the marine transgression at ca. 11-10 cal ka B.P. This new evidence is invaluable for better understanding late Quaternary sedimentary and erosional episodes that characterized the easternmost part of the norther Adriatic Sea, in the frame of the well-known glacio-eustatic sea-level changes.

1. Introduction

The sedimentary response to high-amplitude, late Quaternary glacio-eustatic sea-level changes is commonly recorded along continental margins below shallow shelf areas, especially where subsidence rates are high enough to clearly differentiate marine and continental sedimentation characterizing transgressive-highstand and forced regressive-lowstand deposition, respectively (e.g., Ridente and Trincardi, 2005; Berné et al., 2007; Nordfjord et al., 2009; Maselli et al., 2010, 2011; Schattner et al., 2010). In other cases, glacio-eustasy is recorded by marine terraces along uplifting coasts (e.g., Zazo et al., 2003; Zecchin et al., 2016).

The northern Adriatic Sea (Fig. 1) is a shallow shelf area that is ideal for the study of late Quaternary glacio-eustatic record, as documented mainly along its western margin in the Po River delta and Venice areas (e.g., Amorosi et al., 1999, 2005; Massari et al., 2004; Amorosi and Colalongo, 2005; Zecchin et al., 2008, 2009; Zecchin and Tosi, 2014; Amadori et al., 2020), along its northern margin (see Cerrone et al., 2021 and references therein), as well as offshore of these locations (Zecchin et al., 2017, 2022). Excepting early, preliminary investigations by Albrecht and Mosetti (1987), the mapping of the late Quaternary seafloor stratigraphic sequences (Trincardi et al., 2011), and the Holocene marine sediment distribution (Trobec et al., 2018), the late Quaternary stratigraphy of the eastern part of the northern Adriatic Sea, that is the Trieste Gulf (Fig. 1), was poorly documented. On the other hand, recent studies on the Neogene succession of the Trieste Gulf based on multichannel seismic profiles (Zecchin et al., 2022) show a complex Plio-Pleistocene stratigraphy, but data resolution is not adequate to

* Corresponding author.
E-mail address: mzecchin@ogs.it (M. Zecchin).

https://doi.org/10.1016/j.quaint.2024.03.001
Received 15 December 2023; Received in revised form 8 February 2024; Accepted 1 March 2024
Available online 8 March 2024

document the late Quaternary cyclicity in detail.

The present study aims to document the glacio-eustatic cyclicity in the south-eastern Trieste Gulf area down to a depth of ca. 90 m below present sea level on the basis of high-resolution seismic data and cores, as well as radiocarbon and U-Th dating. Achieving this goal is therefore crucial to cover the present knowledge gap in order to have a clearer picture on the Quaternary evolution of the northern Adriatic Sea, as well as a better understanding of the last interglacial depositional and stratigraphic model.

2. Geological setting

The Trieste Gulf (Fig. 1) is the result of a complex stratigraphic and tectonic evolution. The Mesozoic/Early Cenozoic extensional phase with the deposition of carbonate platform sequences more than 5 km thick (Fantoni et al., 2002; Fantoni and Franciosi, 2010; Busetti et al., 2010a, 2010b; Brancatelli et al., 2023) (Fig. 1) was followed by the Early Cenozoic Dinaric compression. This phase caused the basin flexure with the drowning of the carbonate platforms and consequently the development of a foredeep filled by turbidites mainly during the Eocene. The turbidites consist of silty marls and sandstones and crop out along the eastern and southern coast of the Trieste Gulf, where they are informally referred to as Trieste Flysch (Cucchi et al., 2013) (Fig. 1). In the gulf, the flysch unit beneath the Quaternary sediments exhibits a considerable seismic anisotropy (Picotti et al., 2018), which indicates the same laminated structure typical of the outcropping flysch (Cucchi et al., 2013). The unit under the gulf reaches it maximum thickness of ca. 1.5 km near the eastern coast (Busetti et al., 2010b; Picotti et al., 2018; Dal Cin et al., 2022). The westward propagation of the front of the External Dinarides caused the development of the NW-SE oriented Karst Thrust along the eastern coast of the gulf (Fig. 1), characterized by a vertical throw of more than 1.8 km (Busetti et al., 2010b; Dal Cin et al., 2022), involving the Eocene Trieste Flysch and causing the exposure of the Cretaceous-Paleogene carbonates of the Karst (Cucchi et al., 2013 and references therein).

The Messinian Salinity Crisis, that occurred in the Mediterranean Sea at the end of the Miocene due to a complex interplay between sea level fall, estimated in 800–900 m (Amadori et al., 2018) and compressional tectonics, led to the subaerial exposure of the northern Adriatic. As a result, this area was exposed to erosion and a drainage system developed, with fluvial valleys that incised the bedrock for several hundred meters (Fantoni et al., 2002; Ghielmi et al., 2013; Busetti et al., 2010a; Zecchin et al., 2017, 2022). In the eastern part of the Trieste Gulf, the Messinian erosion produced a prominent unconformity coinciding with the top of the Trieste Flysch (Busetti et al., 2010a, 2010b; Zecchin et al., 2022; Dal Cin et al., 2022).

The marine transgression, accompanied by the deposition of the Pliocene marine sediments in the northern Adriatic (Fantoni et al., 2002; Zecchin et al., 2017, 2022), did not affect the eastern part of the Trieste Gulf, which remained under subaerial conditions until the Early Quaternary (Zecchin et al., 2022). Consequently, the top of the Trieste Flysch is a diachronous erosional surface becoming younger eastward (Zecchin et al., 2022).

The middle-late Quaternary is characterized by glacial and interglacial phases in which an alternation of continental and shallow water sediments accumulated (Giustiniani et al., 2022; Romeo, 2009; Zampa, 2014). During the last glacial period, the south-eastern Trieste Gulf was crossed by the paleofluvial system of the Isonzo, which formed a complex channel levee system (Ronchi et al., 2023). The late Pleistocene-Holocene marine transgression, which was dated in the

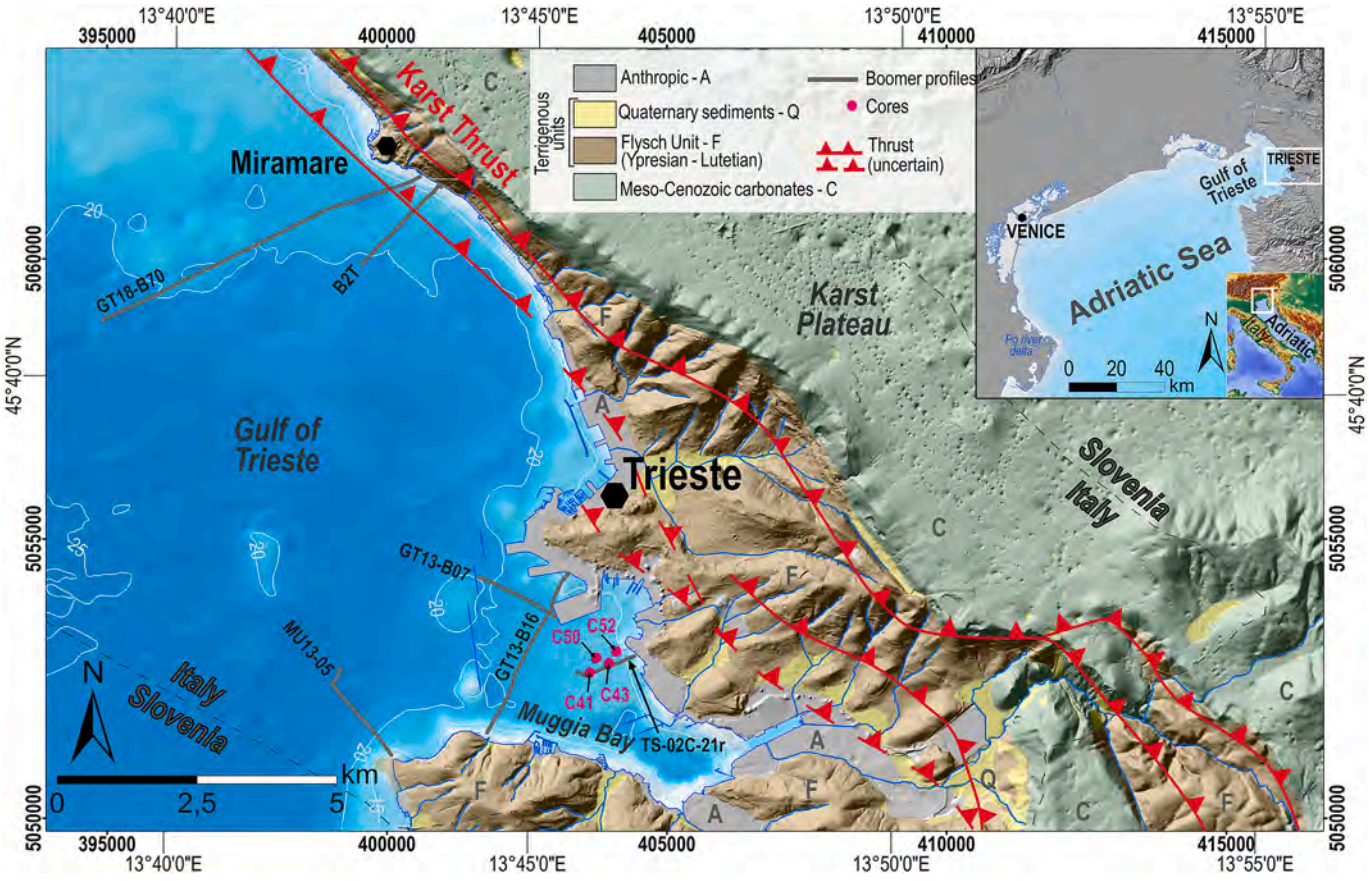

Fig. 1. Location of the study area in the Trieste Gulf, with indicated the studied seismic profiles and sediment cores in the Muggia Bay. On land geology from Cucchi et al. (2013) and digital elevation model (10 m cells) by IRDAT-FVG (2017). Map compiled in ArcGis (Esri). Reference System: datum WGS84, projection UTM33.

eastern part of the Trieste Gulf at about 8800 years ago (Covelli et al., 2006), provides a few thick marine sediments overlying older fluvial channel levee systems (Trobec et al., 2018).

At present, the south-eastern boundary of the Trieste Gulf consists of rocky coasts with narrow gravel and pebble beaches affected by erosion from sea waves and, especially in the south-eastern corner of the Trieste Gulf, forming shore platforms some hundred meters wide at few meters below sea level, together with some 10 m high scarps within the Trieste Flysch (Furlani, 2003; Furlani et al., 2011; Biolchi et al., 2015).

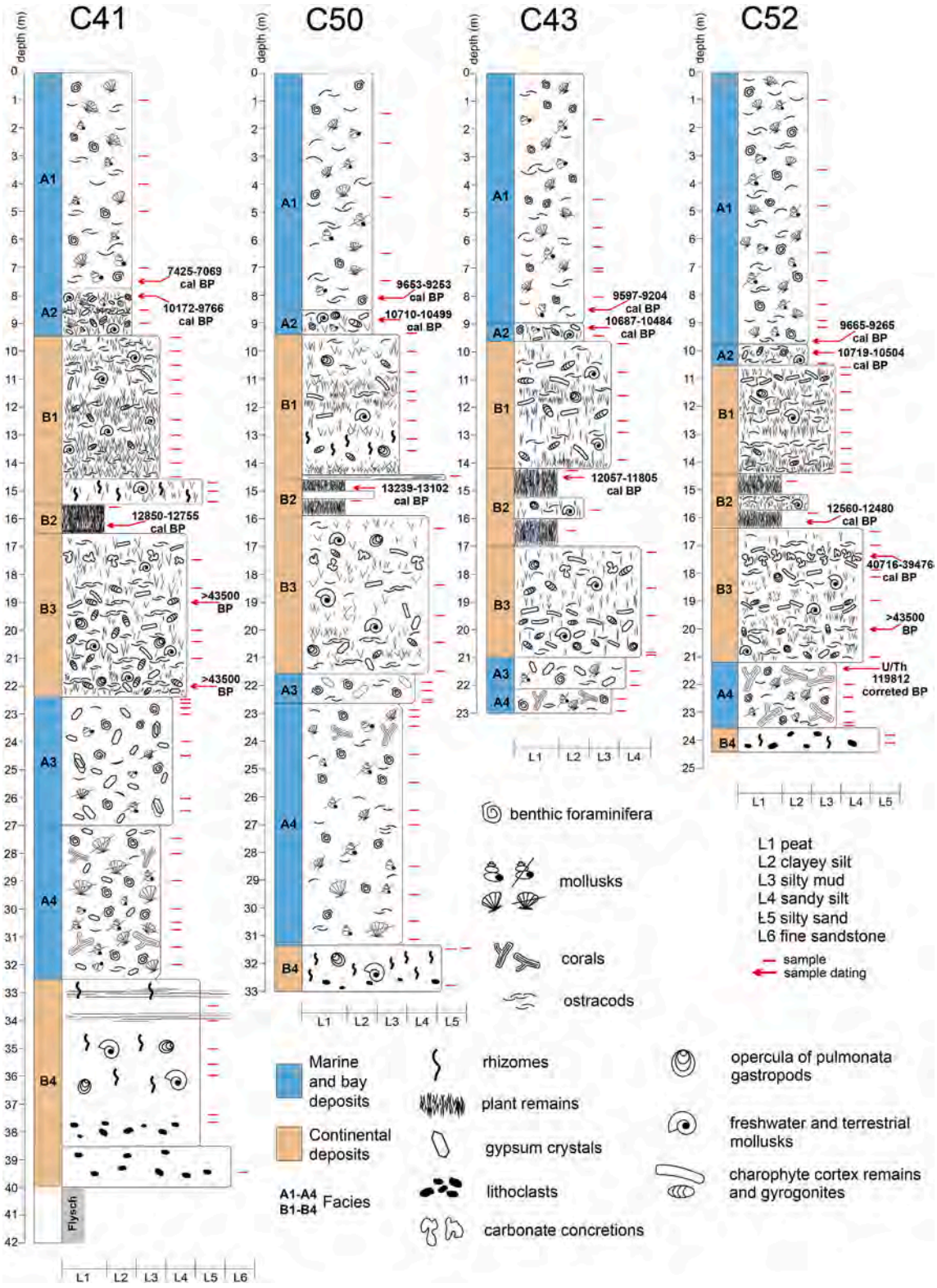

Fig. 2. The four sediment cores analyzed for this study (see Fig. 1 for location). Facies, palaeontologic and lithologic content, samples and datings are indicated. Dating details are reported in Table 1.

3. Methods

The present study was carried out by integrating high-resolution seismic profiles with stratigraphic data from sediment cores (Figs. 1 and 2).

The seismic data used in the present study consists of high-resolution single channel seismic profiles (Fig. 1) belonging to different datasets acquired by OGS:

a) profile B2T acquired in 2003 with a boomer source UWAK 05 by Nautik Nord mounted on a catamaran frame, with 3 shot/second at 300 J, frequency range of 400–7000 Hz;
b) profiles GT13-B07, GT13-B16 and MU13-05, acquired in 2013 with the same UWAK 05;
c) profiles GT18-B70 acquired in 2018 with a boomer source AA301 by Applied Acoustic Engineering (frequency range 400–4000 Hz) mounted on a catamaran frame CAT200, energizing 2 shot/second at 200 J;
d) profile TS-02c-21r acquired in 2021 with a boomer source S-boom (three AA252 plates) by Applied Acoustic Engineering (frequency range 400–3000 Hz) mounted on a catamaran frame energizing 2 shot/second at 300J.

All data were collected with a single trace streamer Geo-Sense Mini-Streamers by Geo-Resources 3 m long (array of 8 hydrophones in oil) using the SB-Logger acquisition system.

The acquisition geometry was parallel: the streamer and the electrodynamic plate are towed in parallel with a lateral offset of a few meters (Baradello and Carcione, 2008).

The profiles were processed using a conventional single-channel sequence: gain recovery (a spherical divergence and balance gain obtained by inverting the amplitude decay curve) and time-variant band-pass filter. Some profiles were acquired in rough seas (sea-waves lifting and lowering the streamer and the plate) resulting in a loss of resolution and thus a loss of reflection continuity. To attenuate this effect, we applied a Non-Surface-Consistent Static Correction that uses a pilot trace (median of the traces sliding along the profile) and a time window on the seafloor to evaluate time shifts with cross-correlation calculations.

Seismic stratigraphic interpretation was done by using the Kingdom™ seismic and geological interpretation software from S&P Global. Time to depth of conversion was calculated using a water velocity of 1530 m/s (Masoli et al., 2015) and a sediment velocity of 1595 m/s (Masoli et al., 2020), both estimated in the Muggia Bay.

Four sediment cores, C41, C43, C50 and C52, were drilled in 2021 by Geosyntech s.r.l. in the Bay of Muggia (Fig. 1) using the pontoon-mounted Puntel PX3 1000 drill with a diameter of 101 mm. The length of the cores ranges from 23 to 42 m below the sea floor.

For the micropaleontological analysis, a total of 156 samples were collected along the entire length of the four cores (55 samples from core C41, 39 samples from core C50, 27 samples from core C43 and 35 samples from core C52). About 50 g of sediment sub-aliquot were picked from each sample to study benthic foraminifera. Samples for foraminifera analyses were dried at 50 °C for 24 h and treated with hydrogen peroxide (10 vol%) for 12 h, later washed through a 125 μm mesh and dried. Subsequently, the sample was weighted and divided into equal fractions using a microsplitter, to obtain sub-samples containing when possible at least 300 specimens of foraminifers, sufficient for identify the dominant taxa, according to Murray (1991). The benthic foraminifera were studied quantitatively under a stereomicroscope Leica S6 D (up to 50x of magnification).

The tables with the relative abundance of the foraminifera as a percentage of each species with respect to the total assemblage present in each sample and the average abundances are available in the supplementary data.

The foraminifera specimens present in the samples were classified following the taxonomic order of Loeblich and Tappan (1987). The environmental interpretation based on the benthic foraminifera assemblages is inferred from the modern benthic communities, following Jorissen (1987), Albani and Serandrei Barbero (1990), Cimerman and Langer (1991), Sgarrella and Moncharmont Zei (1993), Albani et al. (1998), Donnici and Serandrei Barbero (2002), Murray (2006), Milker and Schmiedl (2012) and online catalogues on foraminifera (http s://www.marinespecies.org/index.php and https://foraminifera.eu/).

The chronological framework was provided by sixteen AMS ^{14}C dates (5 from Core C41; 3 from Core C43, 3 from core C50 and 5 from Core C52) obtained from mollusk shells and peat by BETA ANALYTIC Laboratory. Conventional radiocarbon ages were calibrated using the BetaCal 4.20 and the IntCal20 curve (Bronk Ramsey, 2009; Heaton et al., 2020). One U-Th age was obtained by ISOBAR SCIENCE Laboratory from corals collected in core C52 (Table 1). The analysis was performed with the extraction chromatography using Eichron UTEVA resin, followed by multi-collector inductively coupled plasma mass spectrometry (MC-ICP-MS) (Pourmand et al., 2013; Pourmand and Dauphas, 2010), using Thermo Fischer Neptune Plus TM MC-ICP-MS with an Apex-Q desolvation nebulizer.

Powdered samples of 21 samples (in the range 8–37.8 m) from core 41 have been analyzed via X-ray Powder Diffraction at the Department of Mathematics, Informatics and Geosciences of Trieste University using a STOE D 500 X-ray diffractometer at room temperature. The CuKα radiation was used through a flat graphite crystal monochromator. The current used was 20 mA and the voltage was set at 40 kV. The 2θ scanning angle ranged from 2 to 60°, with 0.05° steps and a counting time of 2 s/step.

4. Results

4.1. Sediment cores

Four cores (C41, C43, C50 and C52, Fig. 2) located in the Muggia Bay, south of Trieste (Fig. 1), were analyzed to identify sedimentary facies and microfossil plus mineralogic content, and determine sedimentary environments. Eight facies grouped in two facies associations (A: Marine and bay; B: Continental) were found; their characteristics and environmental significance are described below.

4.1.1. Marine and bay facies association (A)

4.1.1.1. Mollusk-bearing mud (Facies A1). This facies is found in the upper part of all the considered cores and has a thickness ranging from 7.5 to 9.8 m (Fig. 2). It consists of 5Y 5/1 gray clayey silt with a biogenic fraction that includes bivalves (*Chlamys* sp., *Mytilus* sp., venerids and ostreids) and gastropods (*Turritella communis*, *Cerithium vulgatum*, *Nassarius* sp., *Rissoa* sp.), either whole or disarticulated and fragmented (Fig. 2). Microfossils are represented by abundant and well preserved benthic foraminifera, which in all cores form an association that includes *Haynesina germanica* (>27.4% on average), *Ammonia tepida* and *Porosononion granosum* (>20.2% and >16% on average, respectively), and *Elphidium crispum* subordinately (<14%), *Ammonia parkinsoniana* and *Haynesina depressula* (<5%) (supplementary data). Scarce ostracods and spines of echinoids are also present.

4.1.1.2. Ammonia-bearing mud (Facies A2). This facies is found in cores C41 (7.9–9.5 m depth), C43 (9–9.8 m depth), C50 (8.5–9.45 m depth) and C52 (9.8–10.5 m depth) and consists of 5Y 5/1 gray clayey silt with abundant vegetable remains and gyrogonites (calcified fructifications of charophyte) and sparse gypsum crystals (Figs. 2 and 3A). The mollusk association is characterized by either whole or disarticulated and fragmented *Cerastoderma glaucum*, *Bittium reticulatum*, *Gibbula* sp. and *Hydrobia ventrosa* (Fig. 3A). The benthic foraminifera association consists of *A. tepida* (>38.9% on average), *Ammonia parkinsoniana* (>28.8% on average), *H. germanica* (>11.5% on average) and *H. depressula*

Table 1
AMS ^{14}C datings performed on samples from the studied sediment cores, and U-Th geochronology for one coral sample from core C52 (see Fig. 2 for sample location).

AMS ^{14}C datings							
Core	LAT	LONG	Laboratory number	Depth cm	Sample description	Sample code number	Calibrated radiocarbon age (probability 95.4%)
C41	45°37.257′	13°45.970′	Beta-635789	750	Shell (marine)	41-7,50	7425-7069 cal BP
C41	"	"	Beta-635790	800	Shell (freshwater/ terrestrial)	41-8,00	10172-9766 cal BP
C41	"	"	Beta-635791	1625	Peat	41-16,25	12850-12755 cal BP
C41	"	"	Beta-643262	1900	Shell (freshwater/ terrestrial)	41-19,00	>43500 BP
C41	"	"	Beta-643263	2200	Shell (freshwater/ terrestrial)	41-22,00	>43500 BP
C43	45°37.324°	13°46.167′	Beta-635792	850	Shell (marine)	43-8,50	9597-9204 cal BP
C43	"	"	Beta-635793	910	Shell (freshwater/ terrestrial)	43-9,10	10687-10484 cal BP
C43	"	"	Beta-635794	1450	Peat	43-14,50	12057-11805 cal BP
C50	45°37.359′	13°45.982′	Beta-635795	810	Shell (marine)	50-8,10	9653-9253 cal BP
C50	"	"	Beta-635796	890	Shell (freshwater/ terrestrial)	50-8,90	10710-10499 cal BP
C50	"	"	Beta-635797	1490	Peat	50-14,90	13239-13102 cal BP
C52	45°37.437′	13°46.214′	Beta-635798	980	Shell (marine)	52-9,80	9665-9265 cal BP
C52	"	"	Beta-635799	1010	Shell (freshwater/ terrestrial)	52-10,10	10719-10504 cal BP
C52	"	"	Beta-635800	1625	Peat	52-16,25	12560-12480 cal BP
C52	"	"	Beta-643264	1740	Shell (freshwater/ terrestrial)	52-17,40	40716-39476 cal BP
C52	"	"	Beta-643265	2000	Shell (freshwater/ terrestrial)	52-20,00	>43500 BP
U-Th geochronology (coral sample)							
C52	45°37.437′	13°46.214′	IS-1062	2140	coral	52-21,4	119812 corrected BP

subordinately (<5%) (supplementary data). An ostracod association dominated by *Cyprideis torosa* and subordinately *Candona* sp. is also present.

4.1.1.3. Gypsum-bearing sandy silt (Facies A3). This facies is found in three cores, in particular C41 (22.5–27 m depth), C43 (21–22.05 m depth) and C50 (21.55–22.8 m depth) (Fig. 2), and consists of 5Y 4/1 dark gray sandy silt characterized by abundant gypsum crystals and concretions (Figs. 2 and 3B). A mollusk association characterized by *Turritella communis*, *Bittium reticulatum*, *Gibbula albida*, *Rissoa* sp. and *Chlamys* sp. was found. Mollusks are either whole or disarticulated and locally fragmented. The micropaleontological analysis shows a dominance of *A. tepida* (>49% on average) (Fig. 3B) and *A. parkinsoniana* (>30.2% on average), whereas other species, such *as A. beccarii*, *H. germanica* and *P. granosum*, are subordinate (<5%) (supplementary data). The ostracod association is dominated by *Cyprideis torosa*, with scarce *Leptocythere* sp.. Mineralogical analyses on core C41 show variable gypsum content (Fig. 3A). It decreases from 7 to 2% in the interval 26.50–26.00 m, it has a maximum at 23 m (about 9%) and then decreases to 3% at a depth of 22.5 m. In the interval 26–22.50 m, gypsum is associated with a prevalent siliciclastic component (quartz and feldspar).

4.1.1.4. Mollusk and coral-bearing mud (Facies A4). This facies is found in the lower part of all cores, in particular C42 (27–32.5 m depth), C43 (22.05–23 m depth), C50 (22.8–31.2 m depth) and C52 (21.09–23.6 m depth), and consists of 5Y 4/1 dark gray silty mud with very rare gypsum crystals and common either whole or disarticulated and fragmented bivalves (*Cerastoderma glaucum*, *Chlamys* sp., venerids and ostreids) and gastropods (*Aporrhais pespelecani*, *Bolinus* sp., *Nassarius* sp. and *Turritella communis*) (Fig. 2). Abundant hexacorals remains such as *Cladocora caespitosa* are also present (Figs. 2 and 3F). The foraminiferal association is dominated by *A. beccarii*, *A. inflata* and *A. parkinsoniana* (>46% on average) and *E. crispum* subordinately (>13.3% on average) (supplementary data).

4.1.1.5. Interpretation of facies association A. The features of the deposits of facies association A suggest the accumulation in a marine context ranging from open to restricted. In particular, *H. germanica*, *A. tepida* and *P. granosum* found in Facies A1 are generally recorded in shallow shelf environments and bays with relatively low salinity due to freshwater inputs from the land (Albani and Serandrei Barbero, 1990; Donnici and Serandrei Barbero, 2002; Murray, 2006; Melis and Covelli, 2013; Rossi et al., 2021). A shallow-water environment with low salinity is also suggested for Facies A2 due to the presence of gyrogonites, *Candona* sp. and *H. ventrosa*, plus abundant *A. tepida* and *A. parkinsoniana* (Amorosi et al., 2004; Rossi et al., 2021; Žvab Rožič et al., 2022). Also, *H. germanica* suggests freshwater inputs with salinity variations (Melis and Covelli, 2013; Rossi et al., 2021), whereas *C. torosa* is typical of brackish-water and lagoonal environments (Athersuch et al., 1989; Meisch, 2000). On the contrary, the sparse gypsum crystals found in Facies A2 are compatible with a restricted, hypersaline environment (Arenas and Pardo, 1999). It is therefore inferred that Facies A2 accumulated in a relatively restricted bay characterized by strong salinity variations, due to episodes of important freshwater input alternated with others typified by evaporation and gypsum precipitation. A more marked evaporite, marginal-marine or bay environment is inferred for Facies A3 due to the abundance of gypsum. A stressed shallow-water environment for this facies is also indicated by the presence of *A. tepida*, *A. parkinsoniana* and in particular by *C. torosa* (Athersuch et al., 1989; Marocco et al., 1996; Meish, 2000; Donnici and Serandrei Barbero, 2002; Jorissen et al., 2018). The abundance of *A. beccarii* and *A. inflata*, as well as of corals and marine mollusks, strongly suggests that Facies A4 accumulated in a shallow-marine environment, occasionally characterized by relatively low salinity as indicated by the presence of *A. parkinsoniana* (Jorissen, 1988; Sgarrella and Moncharmont Zei, 1993; Fiorini and Vaiani, 2001; Amorosi et al., 2005; Rossi et al., 2021).

4.1.2. Continental facies association (B)

4.1.2.1. Vegetated mud and sand (Facies B1). This facies is found in all cores, in particular C41 (9.5–15.5 m depth), C43 (9.8–14.2 m depth),

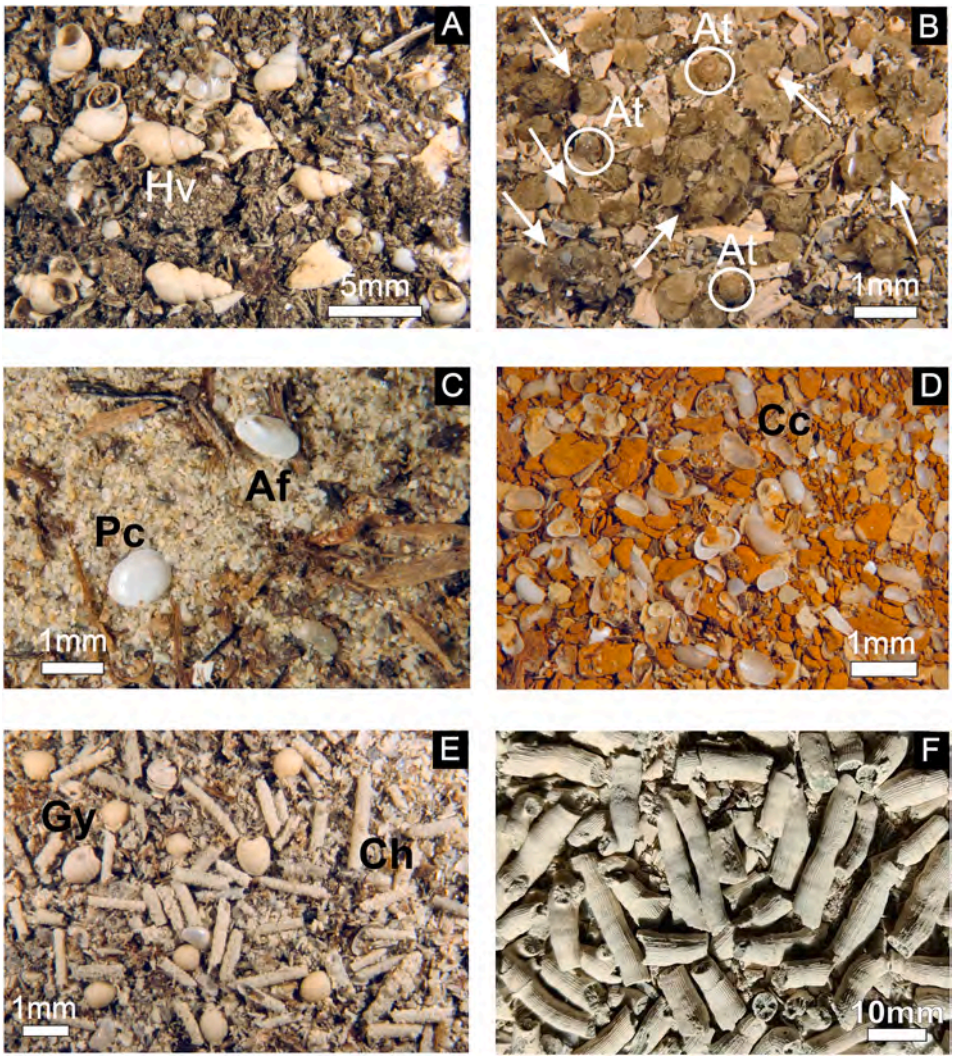

Fig. 3. Microphotographs of the main biogenic content of some facies in the studied cores. (A) Facies A2, sample C41–8.00. *Hidrobia ventrosa* (Hv) with abundant plant remains and ostracods. (B) Facies A3, sample C41–27.30. *Ammonia tepida* (At) and some gypsum crystals indicated by arrow. (C) Facies B1, sample C41–11.10. *Ancylus fluviatilis* (Af) and *Pisidium casertanum* (Pc). (D) Facies B3, sample C52–17.40. Abundant red micritic crusts and concentration of ostracod valves generally of the taxa *Candona candida* (Cc). (E) Facies B3, sample 52–19.10. Calcified remains of a charophyte cortex and calcified fructifications consisting in gyrogonites with a typical spiral structure. (F) Photograph of the Facies A4, sample 52–21.40. Concentration of *Cladocora caespitosa*.

C50 (9.45–14.7 m depth) and C52 (10.5–14.5 m depth), and consists of 5Y 5/2 olive gray (lower part of the facies) to 5Y 5/1 gray (upper part of the facies) silty mud, whereas silty sand composed of sub-rounded quartz grains, arenaceous fragments and micas characterize the lower part of the facies (Fig. 2). Facies B1 contains several layers made up of plant remains with seds, gyrogonites and ostracods (*Candona* sp.) (Fig. 2). Well preserved freshwater mollusks (*Pisidium casertanum*, *Ancylus fluviatilis*) and opercula of pulmonata gastropods are found (Figs. 2 and 3C). Rhizomes, wood fragments and pulmonata gastropods (*Vallonia pulchella*) are also present (Fig. 2).

4.1.2.2. Peat (Facies B2). This facies is found in all cores, in particular C41 (15.5–16.6 m depth), C43 (14.2–17 m depth), C50 (14.7–15.95 m depth) and C52 (14.5–16.45 m depth), and consists of a peat bed made up of an alternation between dense accumulations of vegetable remains and 5Y 3/1 very dark gray clayey mud layers (Fig. 2). Scarce ostracods (*Candona* sp. e *Ilyocipris gibba*), small pulmonata gastropod opercula and gyrogonites are also found (Fig. 2).

4.1.2.3. Charophyte-bearing sandy silt (Facies B3). Facies B3 is found in all cores, in particular C41 (16.6–22.8 m depth), C43 (17–21 m depth), C50 (15.95–21.55 m depth) and C52 (16.45-21-15 m depth), and consists of 5Y 5/1 gray sandy silt containing abundant white micritic crusts and scarce gypsum crystals in the lower part of the facies (Figs. 2 and 3D). Pulmonata gastropods and opercula, generally in fragments, and ostracods (*Candona candida*) are common (Figs. 2 and 3D). Carbonate concretions and red micritic crusts are abundant in the upper part of the facies (between 17 and 18 m depth in all cores) (Fig. 3D), whereas sandy silt layers up to 6 cm thick, alternated with up to 4 cm thick layers containing calcified remains of whitish charophyte tubular cortexes and gyrogonites, are found below (Figs. 2 and 3E).

4.1.2.4. Mud and sand with pulmonata gastropods (Facies B4). This facies is found in the lower part of cores C41 (32.5–40 m depth), C50 (31.2–33 m depth) and C52 (23.6–24.5 m depth) and consists of 5Y 3/1 very dark gray sandy silt containing sub-rounded quartz grains, up to 1 cm wide angular clasts and mica (Fig. 2). In core C41, sand and silt laminae 3–5 cm thick are present in the upper part of the facies, whereas fine-grained quartz sandstone with angular grains and arenaceous fragments up to 2–3 cm wide are present in the lower part (Fig. 2). Locally mineralized wood detritus with up to 2 mm wide grains, rhizome fragments 1–4 mm wide, and sparse reddish micritic crusts, are common

in Facies B4 (Fig. 2). Fragments of pulmonata gastropods (*Halicidae* and *Bithynia* sp.) are also present (Fig. 2).

4.1.2.5. Interpretation of facies association B. The characteristics of the deposits of facies association B suggest the accumulation in a continental setting. In particular, the vegetated silty mud and sand of Facies B1 suggests accumulation adjacent to fluvial channels, such as on levees that experienced alternating floods and drier phases characterized by vegetation growth (e.g., Branß et al., 2022). This interpretation is also confirmed by the presence of freshwater mollusks, such as *Pisidium casertanum* and *Ancylus fluviatilis*, which are typical of these contexts (Soler et al., 2006; Mouthon and Abbaci, 2012). The peat bed of Facies B2, containing freshwater ostracods and pulmonata gastropods, indicates a palustrine environment (e.g., Fubelli et al., 2008). Palustrine areas and ponds are also inferred for Facies B3, as testified by the presence of charophytes and gyrogonites (Kröpelin and Soulié-Märsche, 1991; Soulié-Märsche, 2002). The white micritic crusts, as well as the gypsum crystals found in the lower part of the facies, are inferred to have been produced by precipitation (Platt and Wright, 1992; Arenas and Pardo, 1999), whereas the carbonate concretions and red micritic crusts found in the upper part of the facies are very probably linked to exposure and pedogenesis of the top surface. The presence of terrestrial gastropods, rhizomes, wood detritus and sparse micritic crusts in Facies B4 suggest accumulation in a floodplain experiencing alternating floods and pedogenetic episodes (Miall, 1996; Fisher et al., 2007).

4.1.3. Sediment core dating

Sixteen ^{14}C datings and one U-Th dating were performed in the four studied cores (Table 1 and Fig. 2). These datings have allowed to reconstruct the age framework of the studied deposits, from Facies A1 in the upper part of the cores to Facies A4 down to 21.4 m in core C52 (Fig. 2).

In particular, samples collected in the lower part of Facies A1 (samples 41–7.50, 43–8.50, 50–8.10 and 52–9.80; Table 1) revealed a ^{14}C age ranging between 7069 and 9665 cal ka B.P., in the early Holocene. An earliest Holocene age (between 9766 and 10,719 cal ka B.P.) was determined for Facies A2 (samples 41–8.00, 43–9.10, 50–8.90 and 52–10.10; Table 1). The ^{14}C age of the peat bed of Facies B2 ranges between 11,805 and 13,239 cal ka B.P. (samples 41–16.25, 43–14.50, 50–14.90 and 52–16.25; Table 1) in latest Pleistocene times. A Pleistocene age of 40,716-39,476 cal ka B.P. (sample 52–17.40; Table 1) was determined in the upper part of Facies B3, just below Facies B2, whereas an age exceeding 43,500 cal ka B.P. (upper limit of the ^{14}C method) characterizes the middle to lower part of Facies B3 (samples 41–19.00, 41–22.00 and 52–20.00; Table 1). The marked age difference between Facies B2 and the upper part of Facies B3 (Fig. 2) suggest that a significant hiatus, in the order of ca. 25,000 ka, is associated with the sharp boundary between the two facies.

The U-Th age determined from coral samples collected in the upper part of Facies A4 (sample 52–21.40; Table 1) revealed a corrected age of 119,812 ka B.P., which indicates a Tyrrhenian age (Marine Isotopic Stage, MIS, 5.5). The significance and implications of these datings will be discussed in the next Sections.

4.2. Seismic units

High-resolution seismic profiles allow to recognize seven seismic units down to ca. 120 ms (TWT) (ca. 95 m) (Figs. 4–9). All seismic units terminate landward against a bedrock composed of the Eocene Trieste Flysch (Figs. 1 and 4-9).

4.2.1. The bedrock

The bedrock of the studied seismic units is only locally penetrated by the seismic profiles for ca. 10 ms (TWT) (ca. 8 m). It consists of a tectonized succession affected by mesofolds composed of inclined, undulate and irregular, medium- to high-amplitude reflectors, which are truncated at the top (Figs. 4–9). Chaotic facies are also found locally. The top of the bedrock corresponds to a high-amplitude reflector that exhibits a stepped profile and rises from over 100 ms (TWT) to less than 10 ms (TWT) landwards (i.e., overall to the E in the seismic profiles, and toward the NE and SW margins of the Muggia Bay, Figs. 4–9). The stepped nature of the bedrock top was already observed by Albrecht and

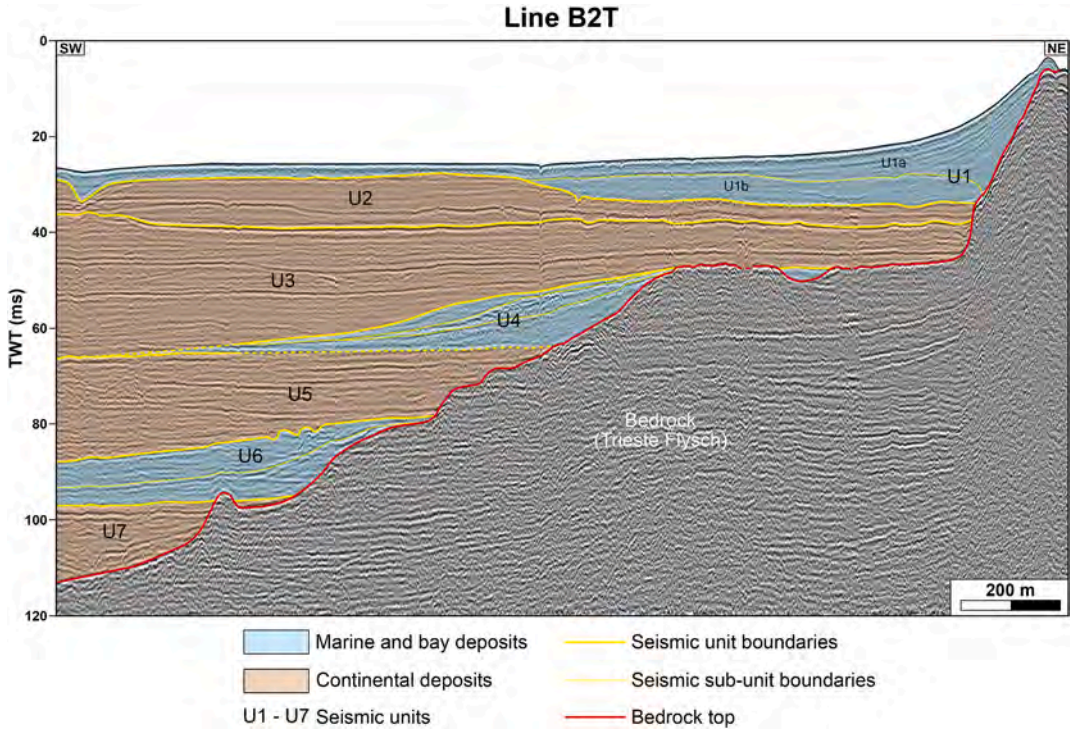

Fig. 4. The B2T high-resolution seismic profile (see Fig. 1 for location). Seismic units and their environmental interpretation (based on recognized features as well as on correlation between cores and Line TS-02C-21r, Fig. 8) are shown.

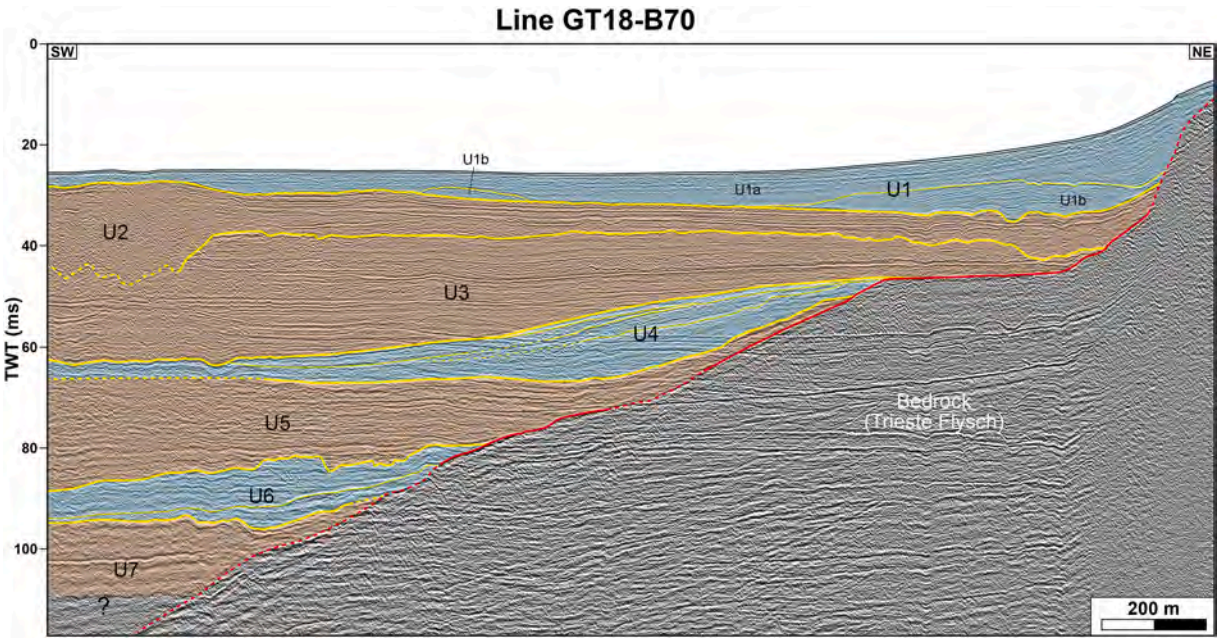

Fig. 5. The GT18-B70 high-resolution seismic profile (see Fig. 1 for location and Fig. 4 for symbols and abbreviations). Seismic units and their environmental interpretation (based on recognized features as well as on correlation between cores and Line TS-02C-21r, Fig. 8) are shown.

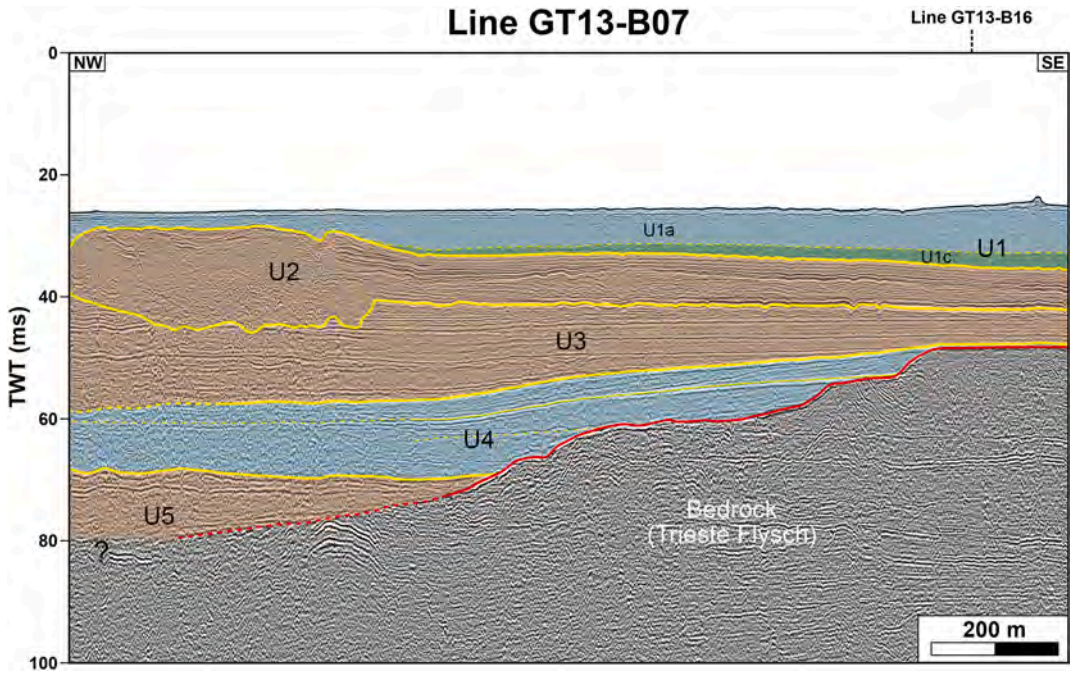

Fig. 6. The GT13-B07 high-resolution seismic profile (see Fig. 1 for location and Fig. 4 for symbols and abbreviations). Seismic units and their environmental interpretation (based on recognized features as well as on correlation between cores and Line TS-02C-21r, Fig. 8) are shown.

Mosetti (1987), Romeo (2009) and Zampa (2014) on the basis of seismic profiles. That surface highlights a major buried terrace between 45 and 50 ms (TWT) (between ca. 35 and 40 m) depth in almost all seismic profiles (Figs. 4–7 and 9), and a minor one between 50 and 55 ms (TWT) (between ca. 40 and 44 m) depth (Figs. 6, 7 and 9). Other buried terraced surfaces are locally found over 80 ms (TWT) (ca. 64 m) depth (Figs. 4 and 9). The major, shallower terrace terminates landward against a prominent buried irregular scarp up to 40 ms (TWT) (ca. 32 m) high, and another buried scarp is locally found between 60 and 80 ms (TWT) depth (Figs. 4, 5, 7 and 9). The seismic units terminate landward against the scarps of the bedrock top and/or may lie on the terraced morphologies defined by the same surface (Figs. 4–9).

4.2.2. Unit 1

Unit 1 is the upper, younger seismic unit of the study area and shows an overall wedge shape, varying in thickness from ca. 2 ms (TWT) (ca. 1.5 m) in relatively distal settings (to the W) to ca. 15 ms (TWT) (ca. 12 m) landwards (Figs. 4–9). It thins further landward, above the shallower buried scarp highlighted by the bedrock top (Figs. 4, 5 and 7-9). The unit overlies Unit 2 and the bedrock in a landward direction and is bounded at the top by the seafloor. Unit 1 shows locally marked thickness changes depending on the morphology of the substrate (Figs. 4–9). In the Trieste

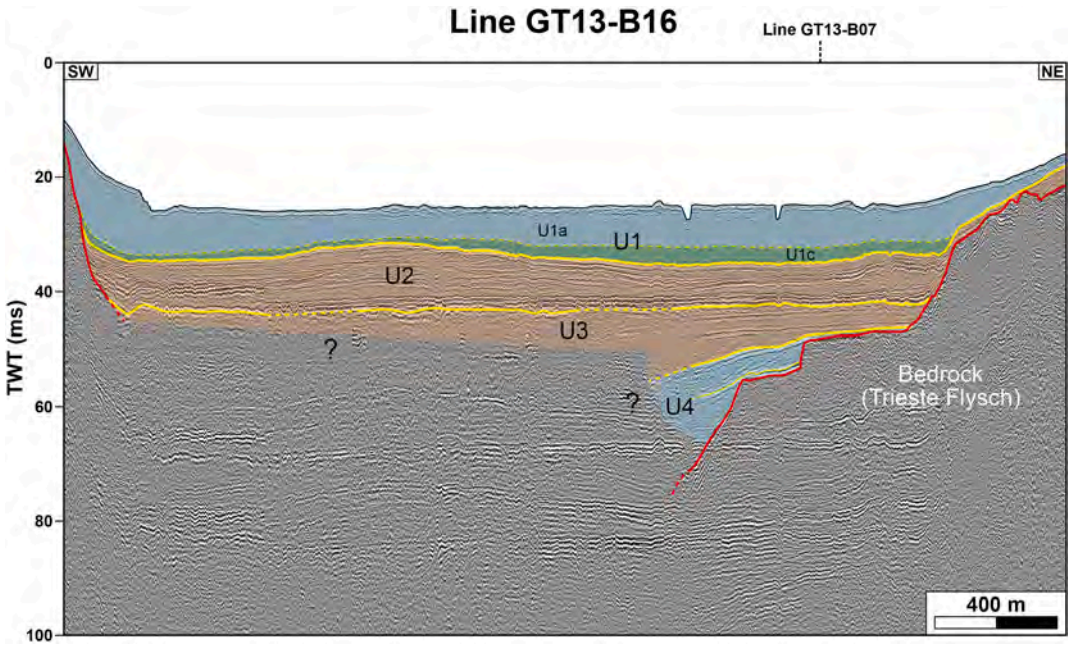

Fig. 7. The GT13-B16 high-resolution seismic profile (see Fig. 1 for location and Fig. 4 for symbols and abbreviations). Seismic units and their environmental interpretation (based on recognized features as well as on correlation between cores and Line TS-02C-21r, Fig. 8) are shown.

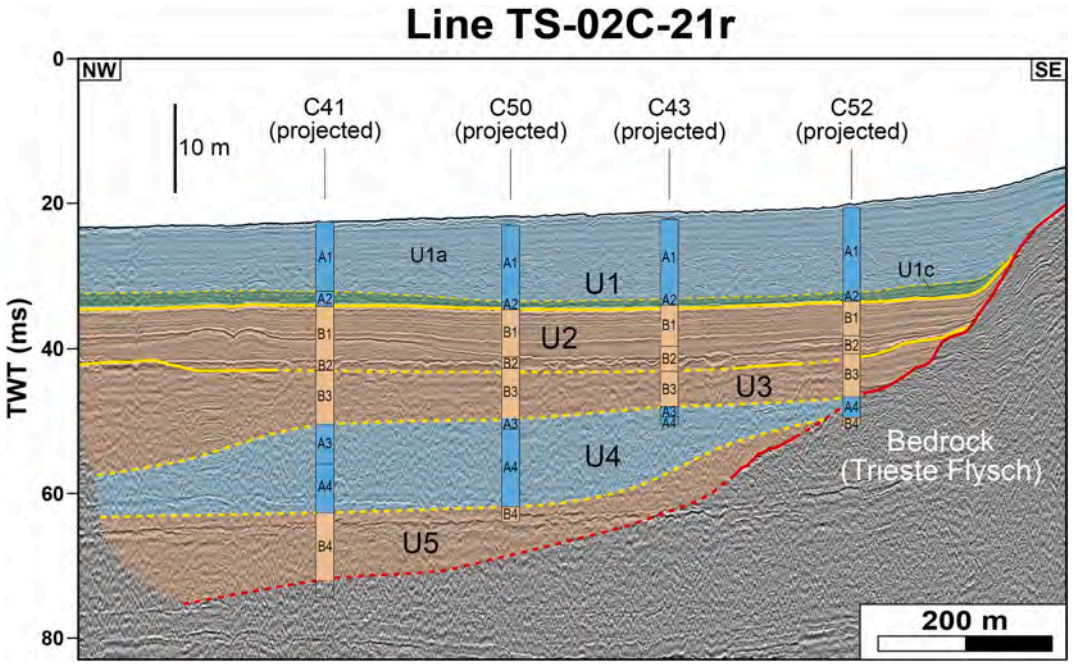

Fig. 8. The TS-02C-21r high-resolution seismic profile (see Fig. 1 for location and Fig. 4 for symbols and abbreviations). Seismic units and their environmental interpretation (based on recognized features as well as on correlation between cores and the present profile) are shown.

Gulf, the base of the unit deepens from ca. 27 ms (TWT) (ca. 21.5 m) to ca. 37 ms (TWT) (ca. 29.5 m) depth landward (to the E), up to the toe of the buried scarp on the bedrock.

Unit 1 is composed of three sub-units (1a, 1b and 1c; Figs. 4–9). Sub-Unit 1a is the upper one and is found in all seismic profiles, showing a progressive thickness increase, up to ca. 15 ms (TWT), landwards (Figs. 4–9). It has transparent seismic facies characterized by generally low-amplitude reflectors that either downlap or onlap the top of Unit 2 or of sub-Unit 1b. The reflectors also either downlap or drape the top of sub-Unit 1c and onlap the bedrock landwards. The reflectors of sub-Unit 1a are gently seaward-inclined near the basin margin, becoming gradually sub-horizontal in relatively distal settings in the Trieste Gulf or in the central part of the Muggia Bay (Figs. 4–9).

Sub-Unit 1b is found only in the Trieste Gulf below the thicker part of sub-Unit 1a and only occasionally in slightly distal settings (Figs. 4, 5 and 9). It consists of convex-up lenticular bodies up to ca. 8 ms (TWT) (ca. 6 m) thick and up to 800 m across, sitting on the top of Unit 2 and the bedrock at their landward termination. Sub-Unit 1b bodies contain low- to medium-amplitude, undulate to inclined sigmoidal reflectors draping the irregular top of Unit 2 in the central part of the subunit, and downlapping or onlapping the top of Unit 2 or of the bedrock toward the peripheral parts. The continuity of these bodies along depositional strike

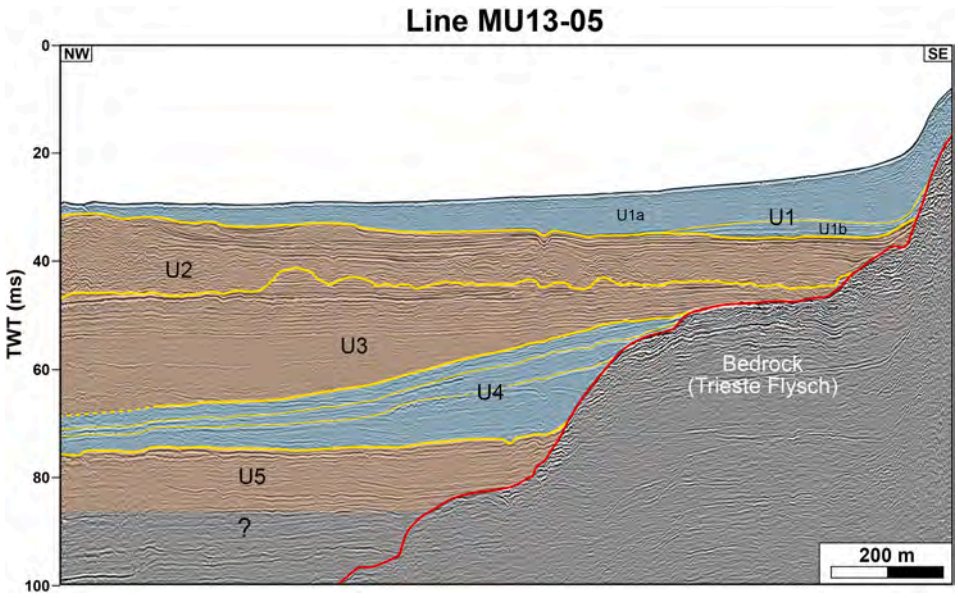

Fig. 9. The MU13-05 high-resolution seismic profile (see Fig. 1 for location and Fig. 4 for symbols and abbreviations). Seismic units and their environmental interpretation (based on recognized features as well as on correlation between cores and Line TS-02C-21r, Fig. 8) are shown.

is uncertain.

Sub-Unit 1c is found only in the Muggia Bay below sub-Unit 1a, where it is continuous (Figs. 6–8). The sub-unit is less than 5 ms (TWT) (4 m) thick and is composed of sub-horizontal to gently-inclined or undulate low-amplitude reflectors that drape the top of Unit 2. The contact between sub-Units 1a and 1c is locally indistinct.

4.2.3. Unit 2

Unit 2 is well recognizable in all seismic profiles between Units 1 and 3 and its thickness varies between ca. 3 and 20 ms (TWT) (between ca. 2.5 and 16 m) (Figs. 4–9). The base of the unit is found between ca. 37 and 50 ms (TWT) (between ca. 29.5 and 40 m) depth and varies between being relatively sub-horizontal and very irregular and concave-up (Figs. 4–9). The top of the unit, coinciding with the base of Unit 1, shows wide, irregular undulations and local, small V- and U-shaped incisions (Figs. 4–9). The unit terminates landward against the bedrock top.

Unit 2 is composed of low- to high-amplitude reflectors that define convex-up bodies ca. 5–10 ms (TWT) (ca. 4–8 m) thick and ca. 400 m to over 1 km across, which stack on each other (Figs. 4–9). These bodies commonly exhibit a small depression at their top where they are thicker, which is repeated in the underlying reflectors (Figs. 4–9). Particularly high-amplitude, sub-horizontal reflectors just overlie the base of the unit in the Muggia Bay (Figs. 6–8). Reflectors of Unit 2 are locally undulate and even chaotic, in particular within the concave-up depressions locally found at the lower boundary of the unit (Figs. 4–9).

4.2.4. Unit 3

Unit 3 is bounded by the irregular base of Unit 2 above and by the top of Unit 4 or the bedrock top below, and its thickness increases seaward (overall to the W) from ca. 3–30 ms (TWT) (ca. 2.5–24 m) (Figs. 4–9). The unit terminates landward against the bedrock top. The lower boundary, between ca. 45 and 67 ms (TWT) (between ca. 36 and 53 m) depth, is seaward inclined and merges landward with the major buried terrace formed by the bedrock top surface (Figs. 4–9). Minor concave-up depressions are locally found along the lower boundary (Fig. 5).

Unit 3 is mainly composed of low- to high-amplitude, sub-horizontal to gently inclined parallel reflectors that onlap the lower boundary, with occasional minor irregular and concave-up reflectors truncating the underlying ones (Figs. 4–9). In places the upper part of the unit is significantly eroded by the top boundary and its parallel reflectors may exhibit angular relationships with those of the overlying Unit 2 (Figs. 5–7 and 9).

4.2.5. Unit 4

Unit 4 is comprised between Unit 3 above and Unit 5 and the bedrock top below (Figs. 4–9). The boundary between Units 4 and 5 is sub-horizontal or either seaward- or landward-inclined, between ca. 50 and 75 ms (TWT) (between ca. 40 and 60 m) depth. Unit 4 is wedge-shaped and thins both seaward (overall to the W) and landward, reaching a maximum thickness of ca. 16 ms (TWT) (ca. 12.7 m) just seaward of the bedrock top (Figs. 4–9). The unit lies just seaward of the major buried terrace formed by the bedrock top between 45 and 50 ms (TWT), and is locally found with minimal thicknesses (ca. 1 ms TWT or a little more) above the terrace itself (Figs. 4–7 and 9). An exception is documented by the correlation between the TS-02C-21r seismic profile and the studied cores in the Muggia Bay, where the terrace on the bedrock seems to be absent (Fig. 8).

Unit 4 is composite, being formed by three to four superimposed wedges up to ca. 5 ms (TWT) (ca. 4 m) thick, composed of low- to medium-amplitude, seaward-inclined sigmoidal to oblique reflectors (Figs. 4–7 and 9). The main surfaces bounding the wedges show gentler seaward inclination and consists of high-amplitude reflectors. The uncertainty on the number of superimposed wedges is due to the mask effect of multiples, especially in the lower part of the unit. The stacking pattern of the individual wedges varies from backstepping in the southern part of the study area, where in some cases they lie on minor terraces at the bedrock top (Figs. 6, 7 and 9), to forestepping or with more complex pattern in the northern part (Figs. 4 and 5).

4.2.6. Unit 5

Unit 5 is comprised between Unit 4 above and Unit 6 plus the bedrock top below, and is up to ca. 23 ms (TWT) (ca. 18 m) thick (Figs. 4–6 and 9). The boundary between Units 5 and 6, between 80 and 88 ms (TWT) (between ca. 64 and 70 m) deep, is very irregular and inclined seaward (overall to the W) (Figs. 4 and 5). Unit 5 is composed of sub-horizontal to gently inclined and locally undulate, low- to high-amplitude reflectors that onlap the lower boundary (Figs. 4–6 and 9). High-amplitude reflectors in the upper part of the unit locally highlight convex-up features with central depressions up to ca. 3 ms (TWT) (ca. 2.4 m) thick, similar to those found in Unit 2 (Fig. 6). The reflectors of the unit can be masked by multiples.

4.2.7. Unit 6

Unit 6 is recognizable only in seismic profiles of the northern part of the study area, between Unit 5 (above) and Unit 7 and the bedrock (below), and shows a wedge shape that thins seaward (to the SW) from ca. 15 to 10 ms (TWT) (from ca. 12 to 8 m) (Figs. 4 and 5). The unit terminates landward against the bedrock top. While the upper boundary can be very irregular (see previous Section), the lower boundary of the unit is ca. 90–97 ms (TWT) (ca. 72–77 m) deep and gently inclined seaward, and it can be locally irregular (Figs. 4 and 5).

Although partially masked by multiples, the reflectors of Unit 6 show low to high amplitude, are seaward inclined with downlap terminations onto the lower boundary, as noted for Unit 4 (Figs. 4 and 5). Some irregularities are found in places along the reflectors. Similarly to what was observed in Unit 4, an higher amplitude reflector represents the boundary between two superimposed wedges, as suggested also by the local presence of seaward-inclined, low-amplitude reflectors that terminate below the high-amplitude ones (Figs. 4 and 5).

4.2.8. Unit 7

Unit 7 is recognizable only in seismic profiles of the northern part of the study area, between Unit 6 (above) and the bedrock (below), whereas its lower boundary in more seaward (to the SW) locations is not recognizable in the present data (Figs. 4 and 5). Unit 7 thickens seaward at least up to ca. 15 ms (TWT) (ca. 12 m) in the available seismic profiles.

The unit is composed of low- to high-amplitude sub-horizontal to gently seaward inclined reflectors, showing local undulations and stepped trends (Figs. 4 and 5).

4.3. Correlation between cores and seismic units and environmental interpretation

The studied cores are very close to the TS-02C-21r seismic profile in the Muggia Bay and near the GT13-B07 and GT13-B16 seismic profiles (Figs. 1 and 8). Subtracting the thickness of the water column from the depths of the seismic lines allows for a precise correlation between facies recognized in the cores and seismic units that was extended to the whole study area.

In particular, sub-Units 1a and 1c correspond to Facies A1 and A2, respectively (Fig. 8); this means that sub-Unit 1a coincides with a Holocene shallow shelf depositional unit showing minor seaward progradation, whereas sub-Unit 1c testifies sedimentation in a restricted bay, early Holocene in age, the area of which corresponded to that of the present day Muggia Bay (Section 4.1.1.5). The characteristics of sub-Unit 1b (Figs. 4, 5 and 9), which is not penetrated by cores, suggest it accumulated as a sediment drift adjacent to the shallow scarp highlighted by the bedrock top (e.g., Stoker et al., 1998) prior to the deposition of the prograding sub-Unit 1a, during a phase characterized by circulation parallel to the scarp.

The convex-up bodies with small depressions at their top found in Unit 2 strongly suggest the aggradation of leveed channels corresponding to Facies B1 (Fig. 8), which was interpreted in the same way (Section 4.1.2.5). The sub-horizontal high-amplitude reflectors that just overlie the boundary between Units 2 and 3 in the Muggia Bay correspond to the relatively thick peat bed of Facies B2, which is therefore considered as part of Unit 2 (Fig. 8). This implies that Unit 2 is latest Pleistocene to earliest Holocene in age, as the overlying sub-Unit 1c (i.e. Facies A2) seems not to reach the base of the Holocene (Section 4.1.3 and Fig. 2). Unit 3, which is mainly composed of sub-horizontal to gently-inclined parallel reflectors, is fully equated to the palustrine deposits of Facies B3, which is pedogenized at its top (Section 4.1.2.5) (Fig. 8). The correlation between Unit 2 and Facies B1 plus Facies B2, and between Unit 3 and Facies B3, implies that the flat to locally incised boundary between Units 2 and 3 is associated with the ca. 25 ka hiatus found between Facies B2 and B3 (Section 4.1.3; Fig. 2); such a surface is therefore to be considered as the main unconformity in the studied Pleistocene-Holocene succession.

The composite, wedge-shaped Unit 4 suggests the progradation of a clastic shallow-marine system, which should be equivalent to the open to restricted marine Facies A4 plus Facies A3 (Fig. 8). Unit 4, therefore, would be Tyrrhenian in age (Section 4.1.3; Fig. 2). The boundary between Facies A3 and Facies A4 could correspond to the lower boundary of the uppermost minor wedge among those composing the main wedge of Unit 4, at least in the Muggia Bay.

The above considerations also suggest a correspondence between Unit 5 and the floodplain deposits of Facies B4 (Fig. 8), whereas a comparability is proposed between the wedge-shaped Unit 6 plus the underlying Unit 7 (Figs. 4 and 5), which are not penetrated by cores, and Units 4 plus Unit 5, respectively.

5. Depositional systems and sequence stratigraphy

5.1. Depositional model

The integrated analysis of seismic profiles and sediment cores indicates that the studied Pleistocene to Holocene succession consists of alternating continental (Units 2, 3, 5 and 7) and marine (Units 1, 4 and 6) depositional systems, which accumulated against a stepped paleoscarp developed on the Eocene Trieste Flysch (Figs. 4–9). This scenario implies the occurrence of three main transgressive-regressive events, associated with the observed alternating continental and marine deposition.

The evidence that the wedge of Unit 4 (Facies A3 and A4) prograded just seaward of the major buried terrace found between 45 and 50 ms (TWT) (between ca. 35 and 40 m) depth, suggests a depositional model similar to that of the Holocene clinoform of the Trieste Gulf (sub-Unit 1a), which prograded starting from the shallower buried scarp highlighted by the bedrock top, and defines a transitional zone between shoreface (landward of the buried scarp) and shelf environments (e.g., Pomar and Tropeano, 2001; Zecchin et al., 2010) (Figs. 4–9). It is therefore likely that the buried terrace between 45 and 50 ms (TWT) depth developed due to wave action as a wave-cut platform, during an episode of relative sea-level rise, leading to the progressive recession of a paleo-coastal cliff (i.e., the shallower buried scarp) and the concomitant accumulation of clastic sediment that formed Unit 4 just seaward of the terrace, some hundreds of meters from the paleo-shoreline at the toe of the cliff (Fig. 10). In particular, cliff retreat likely occurred close to the final stage of transgressive phases, characterized by lower rates of relative sea-level rise to relative sea-level stillstand, whereas during episodes of rapid relative sea-level rise, wave action has not enough time to deeply erode the substrate (Zecchin et al., 2011, 2015, 2019) (Fig. 10). Such a depositional model resembles that of the submerged depositional terraces (SDT; Chiocci et al., 2004; Massari and Chiocci, 2006) or infralittoral prograding wedges (IPW; Hernández-Molina et al., 2000), which accumulated by downwelling storm currents below storm wave base on the wave-ravinement surface (WRS; Swift, 1968; Zecchin et al., 2019 and references therein) (Fig. 10). In particular, SDTs/IPWs prograded during episodes of slowing down in relative sea-level rise punctuating overall transgressive events, such as the post-Last Glacial Maximum (LGM; about 20 ka B.P.) transgression, and trend parallel to the shoreline along narrow and steep shelves (Hernández-Molina et al., 2000; Chiocci et al., 2004; Massari and Chiocci, 2006; Casalbore et al., 2010; Romagnoli et al., 2013; Quartau et al., 2014). Prograding wedges accumulated during transgressive phases, similar to those illustrated in the present study, were also shown by Maselli et al. (2011) and Pellegrini et al. (2015) in the central Adriatic Sea.

In the present case, the prograding wedge of Unit 4 is inferred to have accumulated above a relic paleo-coastal cliff (Figs. 4–7, 9 and 10), drowned and partially eroded by the WRS during transgression (e.g., Zecchin et al., 2015), and was fed by sediment bypassed offshore during the formation of the wave-cut platform and cliff recession. Where the wave-cut platform is absent possibly due to local sheltered conditions preventing intense wave action, such as shown by the correlation

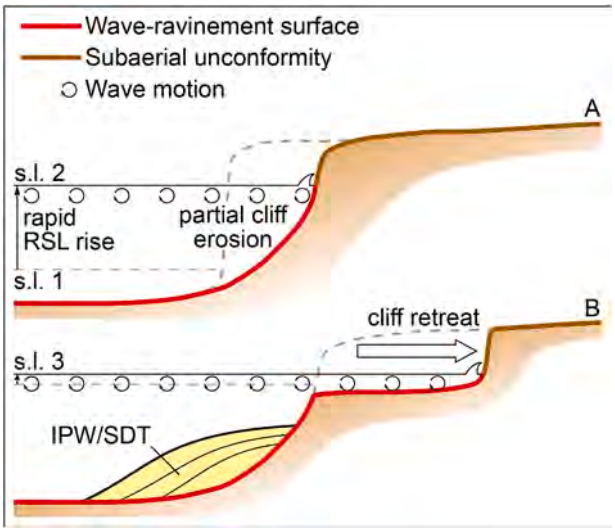

Fig. 10. Model for the development of wave-cut platforms, cliff retreat and the accumulation of subaqueous clastic wedges in high-gradient coastal settings (modified from Zecchin et al., 2019). (A) During episodes of relatively rapid relative sea-level rise, wave action has not enough time to completely dismantle older cliffs and other features on the seafloor. (B) During episodes of relatively slow relative sea-level rise, a wave-cut platform and a receding cliff developed landwards, whereas an infralittoral prograding wedge (IPW), also known as submerged depositional terrace (SDT), starts to accumulate below storm wave base seaward of the platform.

between the TS-02c-21r seismic profile and the studied cores (Fig. 8), the terrace itself is replaced by the flat top of Unit 4, sitting seaward of the buried paleo-coastal cliff. The hypersaline conditions associated with restricted circulation and consequent accumulation of Facies A3 could be unique to the Muggia Bay, where the studied cores are located (Figs. 1 and 2), and they might have occurred in a context of relative sea-level stillstand at the end of the phase of relative sea-level rise.

Where the minor wedges composing Unit 4 show a backstepping stacking pattern (southern part of the study area), their landward parts lie on minor terraces on the bedrock, documenting a stepwise landward retreat of the depositional system (Figs. 6, 7 and 9). Where the minor wedges show a forestepping or more complex stacking pattern, only the main terrace is visible landward, although minor terraces locally developed on Unit 5 (Figs. 4 and 5). In contrast to Unit 4, only a minor buried terrace is locally found landward of Unit 6 (Fig. 4), and this probably reflects an accumulation of the wedge of Unit 6 just seaward of the associated paleo-shoreline.

Regarding the continental deposits of Units 2, 3, 5 and 7 (Figs. 4–9), they document prevailing aggradation of floodplain, palustrine and fluvial sediments with minor fluvial incision. Marked fluvial incision and extensive pedogenesis on interfluves are documented only at the top of Unit 3 (Facies B3) (Figs. 5, 6 and 9), and they are related to the already mentioned unconformity associated with a ca. 25 ka hiatus. In Unit 2, only the peat bed at its base (Facies B2; Fig. 2) reveals the development of paludal conditions with minor sediment supply after the long-lasting phase of sediment cut-off that led to the formation of the main unconformity (e.g., Shanley and McCabe, 1994), whereas the remaining part of the unit testifies marked sediment accumulation and aggradation of fluvial systems before the Holocene marine transgression (Figs. 4–9). A marked unconformity similar to that found between Units 2 and 3 has not been recognized within Units 5 and 7, although local fluvial erosion at the expense of the upper part of the marine Unit 6 is locally observed (Figs. 4 and 5). In contrast, the top of Unit 4 shows only local minor erosional features and in general is well preserved, suggesting it was onlapped and buried by Unit 3 without significant erosional episodes (Figs. 4–7 and 9).

5.2. Sequence stratigraphic architecture

Since the studied succession contains shallow-marine and bay deposits, as well as continental deposits likely accumulated far from the shoreline, the application of traditional sequence stratigraphic models becomes difficult, as fully continental settings in inland areas are not sensitive to relative sea-level changes, rather to local tectonics and climate (Posamentier and Allen, 1999; Catuneanu, 2006). For this reason, a simpler sequence stratigraphic classification, consisting of (1) transgressive/highstand deposits, and (2) forced regressive/lowstand deposits, is adopted here (Fig. 11).

Transgressive/highstand deposits mostly reflect shallow-marine and bay sedimentation in the studied succession and testify stages of relative sea-level rise to stillstand. These deposits are therefore represented by Units 1, 4 and 6 (Figs. 4–9 and 11), which are inferred to be bounded at the base by WRSs possibly merged with maximum regressive surfaces (MRS), or by simple facies contacts below bay deposits, and at the top by subaerial unconformities (SU) recording relative sea-level fall and minor erosion (Fig. 11). The overall good preservation of the shape of the channel-levee systems of Unit 2 suggests that wave action and erosion during the early Holocene marine transgression was scarce, possibly due to sheltered marine conditions (Zecchin et al., 2019), whereas wave power probably increased later along the basin margin during conditions of higher sea level.

The absence of pedogenesis at the top of Facies A3 (upper part of Unit 4; Fig. 8) suggests that the shallow-marine wedge was rapidly buried by the continental Unit 3 (Figs. 4–9). It must be noted that for all marine transgressive/highstand deposits (Units 1, 4 and 6), a separation between a transgressive systems tract and a highstand systems tract is not recognizable (Fig. 11), as the progradation of the subaqueous wedge was concomitant with recession of the paleocliff and shoreline retreat for the whole relative sea-level rise to stillstand stage. This is a common situation in coasts characterized by recessional cliffs and very low sediment supply, so that a highstand normal regression does not start and therefore such coasts should be considered as fully transgressive (e.g., Zecchin et al., 2019); this implies that the prograding Units 1, 4 and 6 can be referred to as transgressive subaqueous healing-phase wedges (Posamentier and Allen, 1999) and that the SU bounding the top of Units 4 and 6 (Fig. 11) is merged with a maximum flooding surface. A possible exception is that documented by the correlation between the TS-02C-21r seismic profile and the studied cores in the Muggia Bay (Fig. 8), where the wave-cut platform has not developed and the progradation of Unit 4, starting from the base of an irregular paleocliff, could at least in part reflect local highstand normal regression.

The sequence stratigraphic model depicted for Unit 4 is also valid for the Holocene clinoform (Unit 1; Fig. 11), as its progradation is concomitant with a recessional to stationary shoreline. In such contexts without or with only occasionally developed highstand normal regressive wedges, and with a very shallow wave-cut platform, a rapid exposure of the whole system at the onset of relative sea-level fall is expected. An indication of onset of relative sea-level lowering might be suggested by the locally recognized forestepping stacking pattern of the minor wedges composing Unit 4 (Fig. 4); however, the local presence of a more complex stacking pattern in this unit, with the last minor wedge that is positioned landwards with respect to the previous one (Fig. 5), plus the dominance of an overall backstepping stacking pattern in other locations (Figs. 6, 7 and 9), suggests that the local forestep of minor wedges in Unit 4 is probably unrelated to relative sea-level lowering but rather to local energy conditions and availability of clastic sediment bypassed offshore during wedge accumulation and cliff retreat.

Given the timing for the formation of the main unconformity separating Units 2 and 3, between 40 and 13 cal ka B.P. (Fig. 2), it very likely developed in fully continental settings across the LGM phase, when the shoreline was far away in the middle Adriatic area (e.g., Trincardi and Correggiari, 2000), and therefore it is inferred to be unrelated to stages of relative sea-level change. The latest Pleistocene to earliest Holocene

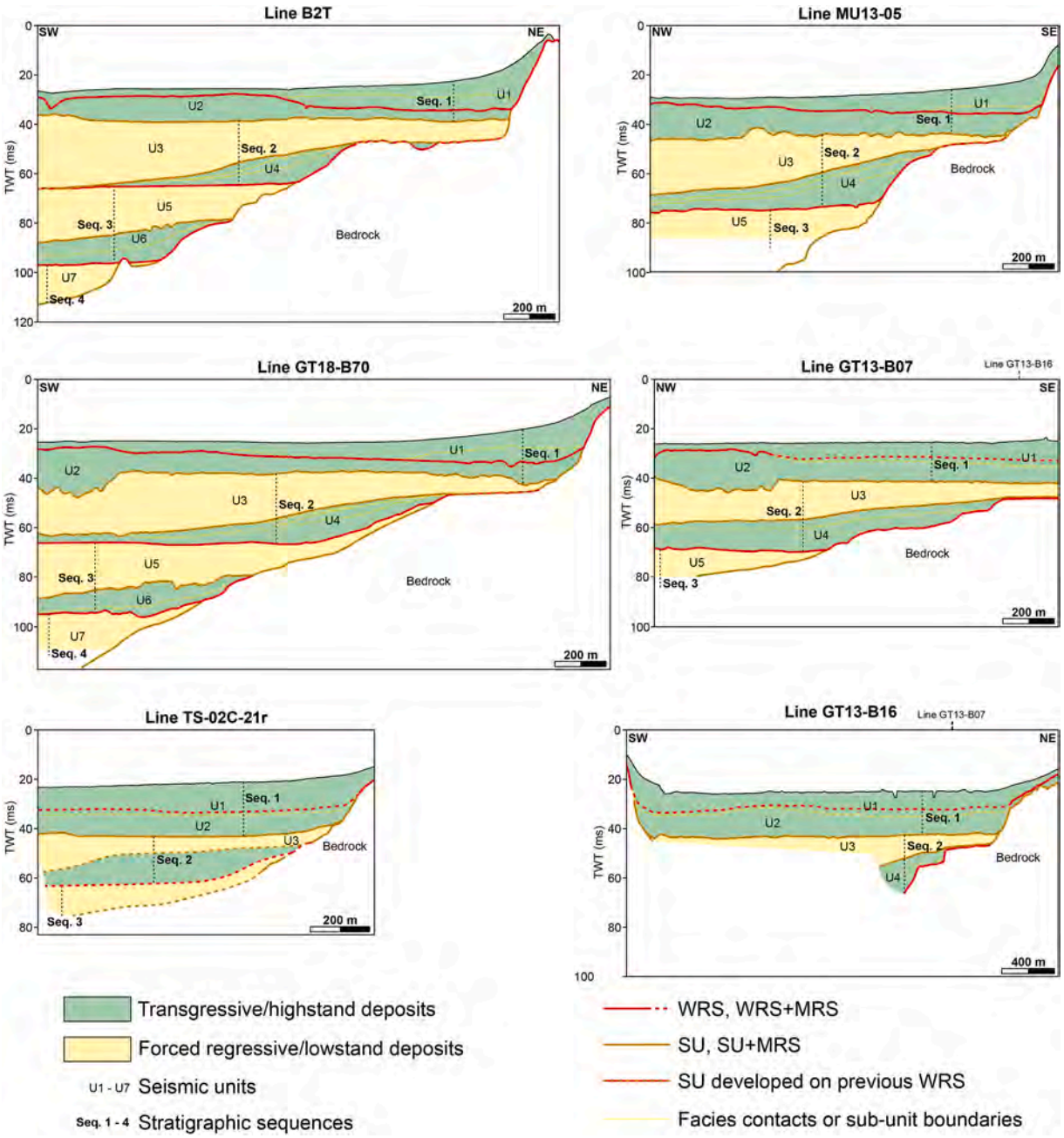

Fig. 11. Sequence stratigraphic interpretation of the studied sedimentary succession, represented by the analyzed seismic profiles. Four sequences, separated by maximum regressive surfaces (merged with either wave-ravinement surfaces or subaerial unconformities) and composed of transgressive/highstand and forced regressive/lowstand deposits, are recognized (see text). Abbreviations: MRS – maximum regressive surface; SU – subaerial unconformity; WRS – wave-ravinement surface.

age of the overlying continental deposits of Unit 2 (Facies B1 and B2; Figs. 2 and 8) suggests that their accumulation, and in particular the aggradation of the recognized fluvial systems, reflected a phase of relative sea-level rise just preceding the Holocene marine transgression in the study area. For this reason, Unit 2 is considered as part of the transgressive/highstand deposits (Fig. 11), and it is inferred to be bounded at the base by the long-lasting subaerial unconformity associated with the main hiatus, merged with a MRS documenting the onset of the latest Pleistocene-Holocene transgressive phase.

In contrast, Units 3, 5 and 7, which do not contain unconformities developed in fully continental settings comparable to that separating Units 2 and 3 (Figs. 4–7 and 9), are inferred to be coeval with forced regressive and lowstand marine deposition (Fig. 11), probably reflecting main glacio-eustatic lowstand phases (e.g., Amorosi et al., 1999; Amorosi and Colalongo, 2005; Zecchin et al., 2009). However, as mentioned above, the fully continental depositional settings characterizing the accumulation of Units 3, 5 and 7 imply that the aggradational architecture of these units is unrelated to any relative sea-level change.

Considering that MRSs documenting the onset of transgressive episodes, merged with either WRSs or the long-lasting SU, are the most common sequence stratigraphic surfaces in the studied succession, they are chosen as boundaries of stratigraphic sequences (Fig. 11), which can be considered as transgressive-regressive (T-R) sequences (Johnson and Murphy, 1984; Embry and Johannessen, 1992). Sequence 1 is therefore composed of Units 1 and 2, and consists of only transgressive/highstand deposits (Fig. 11). Sequence 2 is composed of Unit 4 below

(transgressive/highstand deposits) and Unit 3 above, which is equivalent of forced regressive and lowstand deposits accumulated seaward (Fig. 11). Sequence 3 is composed of Unit 6 and 5, and its architecture is comparable to that of Sequence 2 (Fig. 11). Only the upward and landward part of Sequence 4 is visible in the study area, and it is represented by the continental Unit 7, inferred to be part of forced regressive/lowstand deposits (Fig. 11).

6. Discussion

The present data have allowed to document alternating marine/bay and continental deposits below the Trieste Gulf, composing a stack of transgressive-regressive sequences that testify subsequent cycles of relative sea-level change (Figs. 4–9 and 11). Since the available datings allow to correlate the first marine wedge (Unit 4), found below Holocene and upper Pleistocene marine and continental sediments, with the last interglacial (Tyrrhenian, MIS 5.5) (Figs. 2 and 12), the recognized cyclicity is likely glacio-eustatic in origin. Moreover, despite the prograding wedge of Unit 6 (Figs. 4 and 5) is not penetrated by cores and has not been dated, a correlation of this unit with at least one of the peaks of the penultimate interglacial (MIS 7) is plausible (Fig. 12). These considerations suggest that the stepped profile of the top bedrock surface (e.g., Albrecht and Mosetti, 1987, Romeo, 2009; Zampa, 2014, Figs. 4–9) is the result of alternating phases of wave erosion during marine transgressions, producing terraces and leading to coastal cliff recession, and subaerial exposure before burial by continental sediments during stages of relative sea-level lowering and lowstand (Fig. 11). Similarly to the Holocene marine prograding wedge (Unit 1), in most cases the wedge of Unit 4 is not associated with shoreline regression, rather it documents accumulation of clastics bypassed seaward during the formation of the wave-cut platform and coastal cliff recession (Section 5; Fig. 10).

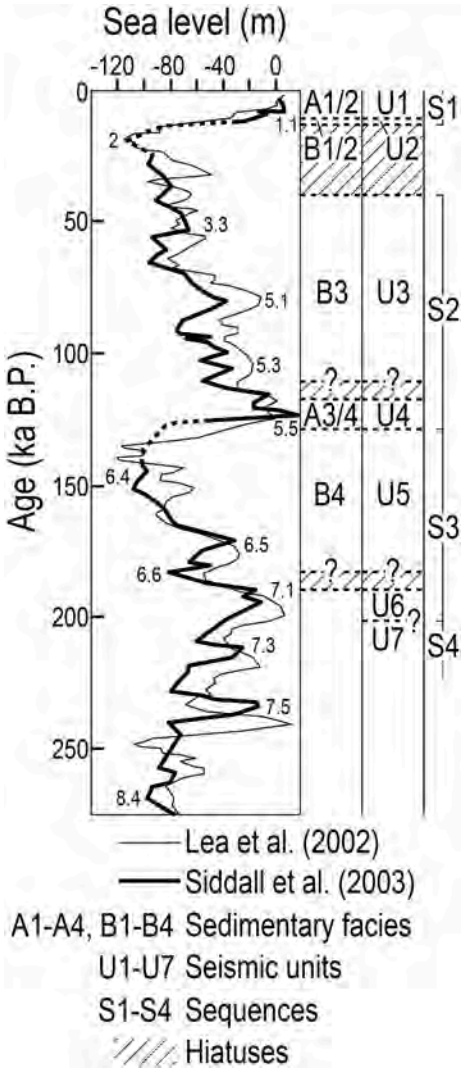

Fig. 12. Chronologic framework of the studied succession based on the sea level curves by Lea et al. (2002) and Siddall et al. (2003) for the last 250 ka, with indication of the Marine Isotope Stages (numbered). Sedimentary facies, seismic units and stratigraphic sequences are reported. The duration of the hiatuses inferred to be associated with the subaerial unconformities bounding the top of seismic Units 4 and 6 (see Fig. 11), as well as the age of Units 6 and 7, are uncertain.

Stacked late Quaternary, glacio-eustatic transgressive-regressive sequences, such as those found in the present study, were already recognized in other locations along the northern Adriatic Sea margin, in particular in the Po river plain (Amorosi et al., 1999; Amorosi and Colalongo, 2005). The main differences between the studied succession and that of the Po river plain is a greater thickness and the absence of buried paleo-coastal cliffs in the latter, implying a faster subsidence (up to 1 mm/a; Ferranti et al., 2006) and a significantly lower coastal gradient along the western margin of the northern Adriatic Sea. In particular, given the available datings (Fig. 2), the depth of the maximum flooding shoreline associated with MIS 5.5 in the study area, inferred to correspond to the landward termination of the buried wave-cut platform behind Unit 4 (Figs. 4–9), is between 45 and 50 ms (TWT) (ca. 35–40 m) depth, whereas the MIS 5.5 shoreline exceeds 100 m of depth in the Po river plain area (Amorosi and Colalongo, 2005), implying a subsidence rate of just one-third (ca. 0.3 mm/a) in the Trieste Gulf. This evidence justifies the very thick (up to ca. 100 m) continental succession separating marine interglacial deposits in the Po river plain area, as well as in the Venice area (Massari et al., 2004; Zecchin et al., 2009), compared to that of the Trieste Gulf.

In the eastern Trieste Gulf, the inferred subsidence rate of ca. 0.3 mm/a since the Tyrrhenian is consistent with the tectonic subsidence calculated from the dating of marine sediments found at archaeological sites in the city of Trieste, which is in the order of 0.2 mm/a since Roman Age (Melis et al., 2012).

Surprising is the recognition of evaporitic gypsum in the upper part of the Tyrrhenian wedge (Facies A3; Fig. 2). The areal extent of hypersaline conditions is uncertain and might be limited to the Muggia Bay, where the studied cores are located (Fig. 1); however, this observation highlights another similarity between the Tyrrhenian and Holocene sedimentation along the coasts of the Trieste Gulf, which is locally suitable to the development of salt marshes.

An unexpected feature found in the studied succession is the unconformity associated with a ca. 25 ka hiatus between Units 2 and 3 (i.e., between Facies B2 and B3; Figs. 2, 8 and 12), largely exceeding the duration of the LGM phase, which has never been recognized in the northern Adriatic area and in the adjacent plain. In comparison, the stratigraphic gap associated with the surface that separates Pleistocene and Holocene deposits in the Venice area ranges from 7 to 13 ka in duration and developed after the LGM (Tosi, 1994; Zecchin et al., 2009). Since the hiatus found in the present study started just after 40 cal ka B.P. and terminated at ca. 13 cal ka B.P. (Figs. 2 and 12), a long-lasting sediment cut-off phase across the LGM characterized at least the southern to central part of the Trieste Gulf. This conclusion contrasts with an inferred active aggradation of the Isonzo megafan NNW of the study area during the LGM phase (Fontana et al., 2014; Ronchi et al., 2023), suggesting that the area toward the SE corner of the Trieste Gulf was outside the Isonzo megafan and was subjected to sediment starvation, pedogenetic processes and local fluvial incision starting from ca. 40 cal ka B.P. The evidence that Unit 3 (Facies B3; Figs. 2 and 8), the accumulation of which predates the formation of the unconformity, is made up of mainly palustrine sediments also suggests a position of the study area away from the main sediment source.

The accumulation of the peat bed of Facies B2 in the Muggia Bay, between ca. 13 and 11.8 cal ka B.P., corresponding to the lowermost part of Unit 2 (Figs. 2, 8 and 12), testifies a marked increase of moisture conditions and vegetation cover above the main unconformity bounding the top of Unit 3, precisely during the Younger Dryas stadial (Rasmussen et al., 2006). These local conditions preceded the onset of marked fluvial aggradation characterizing Unit 2 (Facies B1; Figs. 2 and 8), which were probably associated with a significant increase of sediment supply just at the end of the Younger Dryas stadial (i.e., the beginning of the Holocene at ca. 11.7 cal ka B.P.), before the marine transgression occurred after ca. 11-10 cal ka B.P. (Figs. 2 and 12). Early Holocene continental deposits were recognized also by Covelli et al. (2006) in the eastern Trieste Gulf. Following these considerations, the fluvial aggradation recognized by Ronchi et al. (2023) below the Holocene marine sediments in the Trieste Gulf, corresponding to the aggrading Unit 2 of the present study, must be ascribed to the earliest Holocene rather than the LGM phase.

The present results, therefore, represent an essential step to improve the current knowledge on the Quaternary evolution of the Trieste Gulf area, and more in general of the northern Adriatic Sea, in the frame of the well-known glacio-eustatic cyclicity and related high-magnitude relative sea-level changes.

7. Conclusions

The integrated analysis of high-resolution seismic profiles and core data have allowed to shed new light on the late Quaternary succession of the Trieste Gulf down to ca. 90 m below present sea-level.

The studied succession consists of alternating shallow-marine and continental deposits that compose transgressive-regressive sequences, which terminate landwards against a stepped surface bounding the top of the Trieste Flysch. In particular, seismic data and U-Th datings from cores have allowed to recognize for the first time in the study area Tyrrhenian (MIS 5.5) shallow-marine deposits, which consist of a prograding wedge lying between ca. 40 and 60 m depth, just seaward of a buried wave-cut platform and associated paleo-coastal cliff, and locally containing evaporitic gypsum in its upper part.

The relatively limited thickness of the recognized continental successions, separating marine wedges recording interglacials, indicates an overall lower subsidence rate in this area, in the order of ca. 0.3 m/ka, compared to the western coast of the northern Adriatic Sea.

Remarkable is the recognition of an unconformity associated with a ca. 25 ka stratigraphic hiatus embracing the whole LGM phase, separating pre-LGM palustrine deposits accumulated until ca. 40 cal ka B.P. and a post-LGM peat bed just accumulated during the Younger Dryas stadial between ca. 13 and 11.8 cal ka B.P. These findings testify a relatively long sediment cut-off phase involving at least the southern part of the Trieste Gulf across the LGM, which was not previously recognized. The last marine transgression, occurred since 11-10 cal ka B.P., was preceded by a phase of fluvial aggradation initiated since the beginning of the Holocene.

The present results are relevant to better understand the Quaternary evolution of the Trieste Gulf, improving knowledge on the timing of main sedimentary episodes and on the architecture of depositional systems in the frame of the glacio-eustatic cyclicity.

Data availability

The data that has been used is confidential.

Declaration of competing interest

The authors declare that they have no known competing financial interests or personal relationships that could have appeared to influence the work reported in this paper.

Acknowledgments

The authors would like to thank HHLA-PLT Italy S.r.l. for providing the sediment cores used in this study, Multiproject S.r.l. and Port Network Authority of the Eastern Adriatic Sea (Port of Trieste) for the permission to use the seismic profiles, and S&P Global for providing the educational license of the Kingdom ™ software for the seismic and geological interpretation. The present study was carried out in the frame of the CARG (official geological map of Italy) Project, for the geological mapping at 1:50.000 of the sheets n. 110 Trieste and n. 130 Caresana. The project was funded by the Geological Survey of the Friuli Venezia Giulia Autonomous Region (Italy). We thank two anonymous reviewers and the Editor Jan-Berend Stuut for helpful and constructive comments during the review process.

Appendix A. Supplementary data

Supplementary data to this article can be found online at https://doi.org/10.1016/j.quaint.2024.03.001.

References

Albani, A., Serandrei Barbero, R., 1990. I Foraminiferi della Laguna e del Golfo di Venezia. Memorie Scienze Geologiche Padova 42, 271–341.
Albani, A., Favero, V.M., Serandrei Barbero, R., 1998. Distribution of sediment and benthic foraminifera in the Gulf of Venice, Italy. Estuarine. Coastal and Shelf Science 46, 251–265.
Albrecht, P., Mosetti, F., 1987. Karst evolution and sea level. Memor. Soc. Geol. Ital. 40, 383–387.
Amadori, C., Garcia-Castellanos, D., Toscani, G., Sternai, P., Fantoni, R., Ghielmi, M., Di Giulio, A., 2018. Restored topography of the Po Plain-Northern Adriatic region during the Messinian base-level drop - implications for the physiography and compartmentalization of the palaeo-Mediterranean basin. Basin Res. 30, 1247–1263.
Amadori, C., Ghielmi, M., Mancin, N., Toscani, G., 2020. The evolution of a coastal wedge in response to Plio-Pleistocene climate change: the Northern Adriatic case. Mar. Petrol. Geol. 122, 104675.
Amorosi, A., Colalongo, M.L., Pasini, G., Preti, D., 1999. Sedimentary response to late Quaternary sea-level changes in the Romagna coastal plain (northern Italy). Sedimentology 46, 99–121.
Amorosi, A., Colalongo, M.L., Fiorini, F., Fusco, F., Pasini, G., Vaiani, S.C., Sarti, G., 2004. Palaeogeographic and palaeoclimatic evolution of the Po Plain from 150-ky core records. Global Planet. Change 40, 55–78.
Amorosi, A., Centineo, M.C., Colalongo, M.L., Fiorini, F., 2005. Millennial-scale depositional cycles from the Holocene of the PO plain. Italy. Marine Geology 223–223, 7–18.
Amorosi, A., Colalongo, M.L., 2005. The linkage between alluvial and coeval nearshore marine successions: evidence from the late quaternary record of the Po River Plain, Italy. In: Blum, M.D., Marriott, S.B., Leclair, S.F. (Eds.), Fluvial Sedimentology VII, vol. 35. International Association of Sedimentologists Special Publication, pp. 257–275.
Arenas, C., Pardo, G., 1999. Latest Oligocene–Late Miocene lacustrine systems of the north-central part of the Ebro Basin (Spain): sedimentary facies model and palaeogeographic synthesis. Palaeogeogr. Palaeoclimatol. Palaeoecol. 151, 127–148.
Athersuch, J., Horne, D.J., Whittaker, J.E., 1989. Marine and Brackish Water Ostracods. E.J. Brill, Leiden. Synopses of the British fauna, New Series, p. 343 no. 43.
Baradello, L., Carcione, J.M., 2008. Optimal seismic-data acquisition in very shallow water. Surveys in the Venice lagoon. Geophysics 73 (6), Q59–Q63.
Berné, S., Jouet, G., Bassetti, M.A., Dennielou, B., Taviani, M., 2007. Late Glacial to Preboreal sea-level rise recorded by the Rhône deltaic system (NW Mediterranean). Mar. Geol. 245, 65–88.
Biolchi, S., Furlani, S., Covelli, S., Busetti, M., Cucchi, F., 2015. Morphoneotectonics and lithology of the eastern sector of the Gulf of Trieste (NE Italy). J. Maps 12, 936–946.
Branß, T., Núñez-González, F., Aberle, J., 2022. Fluvial levees in compound channels: a review on formation processes and the impact of bedforms and vegetation. Environ. Fluid Mech. 22, 559–585.
Brancatelli, G., Busetti, M., Dal Cin, M., Forlin, E., 2023. Reprocessing the CROP95-M18 vintage multichannel seismic data acquired in the northern Adriatic Sea: the case of high penetration crustal profile recorded in shallow waters. Bull. GeoPhys. ObServ. 64, 213–236.
Bronk Ramsey, C., 2009. Bayesian analysis of radiocarbon dates. Radiocarbon 51, 337–360.
Busetti, M., Volpi, V., Barison, E., Giustiniani, M., Marchi, M., Ramella, R., Zanolla, C., 2010a. Cenozoic seismic stratigraphy and tectonic evolution of the gulf of Trieste (northern Adriatic). GeoActa SP3 1–14.
Busetti, M., Volpi, V., Nicolich, R., Barison, E., Romeo, R., Baradello, L., Ramella, R., 2010b. Dinaric tectonic features in the gulf of Trieste (northern Adriatic). Bollettino di Geofisica Teorica e Applicata 51 (2–3), 117–128.

Casalbore, D., Romagnoli, C., Chiocci, F.L., Frezza, V., 2010. Morpho-sedimentary characteristics of the volcaniclastic apron around Stromboli volcano (Italy). Mar. Geol. 269, 132–148.
Catuneanu, O., 2006. Principles of Sequence Stratigraphy. Elsevier, Amsterdam, p. 386.
Cerrone, C., Vacchi, M., Fontana, A., Rovere, A., 2021. Last Interglacial sea-level proxies in the western Mediterranean. Earth Syst. Sci. Data 13, 4485–4527.
Chiocci, F.L., D'Angelo, S., Romagnoli, C., 2004. Introduzione. In: Chiocci, F.L., D'Angelo, S., Romagnoli, C. (Eds.), Atlante dei Terrazzi Deposizionali Sommersi Lungo le Coste Italiane. Memorie Descrittive della Carta Geologica d'Italia, vol. 58, pp. 5–8.
Cimerman, F., Langer, M.R., 1991. Mediterranean Foraminifera. Slovenska Akademija Znanosti in Umetnosti, Ljubljana, p. 118.
Covelli, S., Fontolan, G., Faganeli, J., Ogrinc, N., 2006. Anthropogenic markers in the Holocene stratigraphic sequence of the gulf of Trieste (northern Adriatic Sea). Mar. Geol. 230 (1–2), 29–51. https://doi.org/10.1016/j.margeo.2006.03.013.
Cucchi, F., Piano, C., Fanucci, C.F., Pugliese, N., Tunis, G., Zini, L., 2013. Brevi Note Illustrative della Carta Geologica del Carso Classico Italiano. Progetto GEO-CGT, Regione Autonoma Friuli Venezia Giulia, p. 43. Available at: http://www.regione.fvg.it/rafvg/cms/RAFVG/ambiente-territorio/tutela-ambiente-gestione-risorse-naturali/.
Dal Cin, M., Böhm, G., Busetti, M., Picotti, S., Zgur, F., Camerlenghi, A., 2022. 3D P-wave velocity-depth model by means of reflection tomography and depth imaging from multichannel seismic data in the northeastern edge of Adria microplate (Gulf of Trieste, north-eastern Adriatic Sea). Tectonophysics 838, 1–16.
Donnici, S., Serandrei Barbero, R., 2002. The benthic foraminiferal communities of the northern Adriatic continental shelf. Mar. Micropaleontol. 44, 93–123.
Embry, A.F., Johannessen, E.P., 1992. T-R sequence stratigraphy, facies analysis and reservoir distribution in the uppermost TriassicеLower Jurassic succession, western Sverdrup Basin, Arctic Canada. In: Vorren, T.O., Bergsager, E., Dahl-Stamnes, O.A., Holter, E., Johansen, B., Lie, E., Lund, T.B. (Eds.), Arctic Geology and Petroleum Potential, vol. 2. Norwegian Petroleum Society (NPF) Special Publication, pp. 121–146.
Fantoni, R., Catellani, D., Merlini, S., Rogledi, S., Venturini, S., 2002. La registrazione degli eventi deformativi cenozoici nell'avampaese Veneto-Friulano. Memor. Soc. Geol. Ital. 57 (1), 301–313.
Fantoni, R., Franciosi, R., 2010. Tectono-sedimentary setting of the Po plain and Adriatic foreland. Rendiconti Fis. Accademia Lincei 21, 197–209.
Fontana, A., Mozzi, P., Marchetti, M., 2014. Alluvial fans and megafans along the southern side of the Alps. Sediment. Geol. 301, 150–171.
Ferranti, L., Antonioli, F., Mauz, B., Amorosi, A., Dai Pra, G., Mastronuzzi, G., Monaco, C., Orrù, P., Pappalardo, M., Radtke, U., Renda, P., Romano, P., Sansò, P., Verrubbi, V., 2006. Markers of the last interglacial sea level highstand along the coast of Italy: tectonic implications. Quat. Int. 145–146, 30–54.
Fiorini, F., Vaiani, S.C., 2001. Benthic foraminifers and transgressive–regressive cycles in the Late Quaternary subsurface sediments of the Po Plain near Ravenna (Northern Italy). Boll. Soc. Paleontol. Ital. 40, 357–403.
Fisher, J.A., Nichols, G.J., Waltham, D.A., 2007. Unconfined flow deposits in distal sectors of fluvial distributary systems: Examples from the Miocene Luna and Huesca Systems, Northern Spain. Sediment. Geol. 195, 55–75.
Fubelli, G., Falcucci, E., Mei, A., Dramis, F., 2008. Evoluzione quaternaria del Bacino di Leonessa (Rieti). Italian Journal of Quaternary Sciences 21 (2), 457–468.
Furlani, S., 2003. Shore platforms along the North-Western Istrian coast: an overview. Annales - Ser. Hist. Nat. 13 (2), 247–256.
Furlani, S., Biolchi, S., Cucchi, F., Antonioli, F., Busetti, M., Melis, R., 2011. Tectonic effects on late-holocene sea level changes in the gulf of Trieste (NE Adriatic Sea, Italy). Quat. Int. 232, 144–157.
Ghielmi, M., Minervini, M., Nini, C., Rogledi, S., Rossi, 2013. M. Late Miocene-Middle Pleistocene sequences in the Po Plain-Northern Adriatic Sea (Italy): the stratigraphic record of modification phases affecting a complex foreland basin. Mar. Petrol. Geol. 42.
Giustiniani, M., Busetti, M., Dal Cin, M., Barison, E., Cimolino, A., Brancatelli, G., Baradello, L., 2022. Geophysical and geological views of potential water resources in the north-eastern Adriatic Sea. Geosciences 12, 139.
Heaton, T.J., Köhler, P., Butzin, M., Bard, E., Reimer, R.W., Austin, W.E.N., Bronk Ramsey, C., Grootes, P.M., Hughen, K.A., Kromer, B., Reimer, P.J., Adkins, J., Burke, A., Cook, M.S., Olsen, J., Skinner, L.C., 2020. Marine20—the marine radiocarbon age calibration curve (0–55,000 cal BP). Radiocarbon 62, 779–820.
Hernández-Molina, F.J., Fernández-Salas, L.M., Lobo, F., Somoza, L., Díaz del Río, V., Dias, J.M.A., 2000. The infralittoral prograding wedge: a new large-scale progradational sedimentary body in shallow marine environments. Geo Mar. Lett. 20, 109–117.
IRDAT-FVG, 2017. Infrastruttura Regionale di Dati Ambientali e Territoriali per il Friuli Venezia Giulia. Available at: https://irdat.regione.fvg.it/WebGIS/.
Johnson, J.G., Murphy, M.A., 1984. Time-rock model for Siluro-Devonian continental shelf, western United States. GSA Bulletin 95, 1349–1359.
Jorissen, F.J., 1987. The distribution of benthic foraminifera in the Adriatic Sea. Mar. Micropaleontol. 12, 21–48.
Jorissen, F.J., 1988. Benthic foraminifera from the Adriatic Sea; principles of phenotypic variation. Utrecht Micropaleontol. Bull. 37, 1–174.
Jorissen, F., Nardelli, M.P., Almogi-Labin, A., Barras, C., Bergamin, L., Bicchi, E., El Kateb, A., Ferraro, L., McGann, M., Morigi, C., Romano, E., Sabbatini, A., Schweizer, M., Spezzaferri, S., 2018. Developing Foram-AMBI for biomonitoring in the Mediterranean: species assignments to ecological categories. Mar. Micropaleontol. 140, 33–45.
Kröpelin, S., Soulié-Märsche, I., 1991. Charophyte remains from Wadi Howar as evidence for deep mid-Holocene freshwater lakes in the Eastern Sahara (NW Sudan). Quat. Res. 36, 210–223.
Lea, D.W., Martin, P.A., Pak, D.K., Spero, H.J., 2002. Reconstructing a 350 ky history of sea level using planktonic Mg/Ca and oxygen isotope records from a Cocos Ridge core. Quat. Sci. Rev. 21, 283–293.
Loeblich Jr., A.R., Tappan, H., 1987. Foraminiferal Genera and Their Classification. Van Reinhold Company, New York, p. 970.
Marocco, R., Melis, R., Montenegro, M.E., Pugliese, N., Vio, E., Lenardon, G., 1996. Holocene evolution of the caorle barrier-lagoon (norther Adriatic Sea, Italy). Riv. Ital. Paleontol. Stratigr. 102, 385–396.
Maselli, V., Trincardi, F., Cattaneo, A., Ridente, D., Asioli, A., 2010. Subsidence pattern in the central Adriatic and its influence on sediment architecture during the last 400 kyr. J. Geophys. Res. 115, B12106.
Maselli, V., Hutton, E.W., Kettner, A.J., Syvitski, J.P.M., Trincardi, F., 2011. High-frequency sea level and sediment supply fluctuations during Termination I: an integrated sequence-stratigraphy and modeling approach from the Adriatic Sea (Central Mediterranean). Mar. Geol. 287, 54–70.
Masoli, C.A., Petronio, L., Gordini, E., Deponte, M., Cotterle, D., Romeo, R., Böhm, G., Barbagallo, A., Belletti, R., Maffione, S., Meneghini, F., 2015. Marine geophysical investigations in support to the construction of the new harbor infrastructure: the Trieste Marine Terminal extension. Proceedings of the 34 GNGTS Congress, Trieste 63–70, 17-19 November 2015.
Masoli, C.A., Petronio, L., Gordini, E., Deponte, M., Boehm, G., Cotterle, D., Romeo, R., Barbagallo, A., Belletti, R., Maffione, S., Meneghini, F., Baradello, L., 2020. Near-shore geophysical and geotechnical investigations in support of the Trieste Marine Terminal extension. Near Surf. Geophys. 18, 73–89.
Massari, F., Rio, D., Serandrei Barbero, R., Asioli, A., Capraro, L., Fornaciari, E., Vergerio, P.P., 2004. The environment of Venice area in the past two million years. Palaeogeogr. Palaeoclimatol. Palaeoecol. 202, 273–308.
Massari, F., Chiocci, F., 2006. Biocalcarenite and mixed cool-water prograding bodies of the Mediterranean Pliocene and Pleistocene: architecture, depositional setting and forcing factors. In: Pedley, H.M., Carannante, G. (Eds.), Cool-water Carbonates: Depositional Systems and Palaeoenvironmental Controls, vol. 255. Geological Society Special Publication, pp. 95–120.
Meish, C., 2000. Freshwater ostracoda of western and central Europe. In: Schwoerbel, J., Zwick, P. (Eds.), Süesswasserfauna von Mitteleuropa. Spektrum Akademischer Verlag, Heidelberg, Berlin, p. 522, 8/3.
Melis, R., Covelli, S., 2013. Distribution and morphological abnormalities of recent foraminifera in the marano and grado lagoon (north Adriatic Sea, Italy). Mediterr. Mar. Sci. 14/2, 432–450.
Melis, R., Furlani, S., Antonioli, F., Biolchi, S., Degrassi, V., Mezgec, K., 2012. Sea level and paleoenvironment during roman times inferred from coastal archaeological sites in Trieste (northern Italy). Alpine and Mediterranean Quaternary 25 (1), 41–55, 2012.
Miall, A.D., 1996. The Geology of Fluvial Deposits: Sedimentary Facies, Basin Analysis, and Petroleum Geology. Springer, Berlin, p. 582.
Milker, Y., Schmiedl, G., 2012. A taxonomic guide to modern benthic shelf foraminifera of the western Mediterranean Sea. Palaeontol. Electron. 15 (2), 134p, 16A.
Mouthon, J., Abbaci, K., 2012. The taxonomic confusion surrounding Pisidium (Bivalvia, Sphaeriidae): the possible birth of a new taxon. Basteria 76 (4–6), 126–130.
Murray, J.W., 1991. Ecology and Paleoecology of Benthic Foraminifera. Longman Scientific & Technical, Essex (UK), p. 397.
Murray, J.W., 2006. Ecology and Applications of Benthic Foraminifera. Cambridge University Press, New York, p. 426.
Nordfjord, S., Goff, J.A., Duncan, L.S., Austin, J.A., 2009. Shallow stratigraphy and transgressive ravinement on the New Jersey shelf: implications for sedimentary lobe deposition and latest Pleistocene-Holocene sea level history. Mar. Geol. 266, 232–243.
Pellegrini, C., Maselli, V., Cattaneo, A., Piva, A., Ceregato, A., Trincardi, F., 2015. Anatomy of a compound delta from the post-glacial transgressive record in the Adriatic Sea. Mar. Geol. 362, 43–59.
Picotti, S., Dal Cin, M., Böhm, G., Busetti, M., 2018. Evidences of seismic flysch anisotropy in the gulf of Trieste. In: 24th European Meeting of Environmental and Engineering Geophysics, pp. 1–5. https://doi.org/10.3997/2214-4609.201802637. Sep. 2018.
Platt, N.H., Wright, V.P., 1992. Palustrine carbonates at the Florida Everglades: towards an exposure index for the freshwater environment. J. Sediment. Petrol. 62, 1058–1071.
Pomar, L., Tropeano, M., 2001. The Calcarenite di Gravina Formation in Matera (southern Italy): new insights for coarse-grained, large-scale, cross-bedded bodies encased in offshore deposits. AAPG Bulletin 85, 661–689.
Posamentier, H.W., Allen, G.P., 1999. Siliciclastic sequence stratigraphy e concepts and applications. In: SEPM Concepts in Sedimentology and Paleontology, vol. 7, p. 210.
Pourmand, A., Dauphas, N., 2010. Distribution coefficients of 60 elements on TODGA resin: application to Ca, Lu, HF, U and Th isotope geochemistry. Talanta 81, 741–753.
Pourmand, A., Tissot, F.L.H., Arienzo, M., Shafir, A., 2013. Introducing a comprehensive data reduction and uncertainty propagation algorithm for U-Th geochronometry with extraction chromatograpfy and isotope dilution MC-IC-MS. Geostand. Geoanal. Res. https://doi.org/10.1111/j.1751-908X.2013.00266.x.
Quartau, R., Hipólito, A., Romagnoli, C., Casalbore, D., Madeira, J., Tempera, F., Roque, C., Chiocci, F.L., 2014. The morphology of insular shelves as a key for understanding the geological evolution of volcanic islands: insights from Terceira Island (Azores). G-cubed 15, 1801–1826.

Rasmussen, S.O., Andersen, K.K., Svensson, A.M., Steffensen, J.P., Vinther, B.M., Clausen, H.B., Siggaard-Andersen, M.-L., Johnsen, S.J., Larsen, L.B., Dahl-Jensen, D., Bigler, M., Röthlisberger, R., Fischer, H., Goto-Azuma, K., Hansson, M.E., Ruth, U., 2006. A new Greenland ice core chronology for the last glacial termination. J. Geophys. Res. 111, D06102 https://doi.org/10.1029/2005JD006079.

Ridente, D., Trincardi, F., 2005. Pleistocene "muddy" forced-regression deposits on the Adriatic shelf: a comparison with prodelta deposits of the late Holocene highstand mud wedge. Mar. Geol. 222–223, 213–233.

Romagnoli, C., Casalbore, D., Bosman, A., Braga, R., Chiocci, F.L., 2013. Submarine structure of Vulcano Volcano (Aeolian Islands) revealed by high-resolution bathymetry and seismo-acoustic data. Mar. Geol. 338, 30–45.

Romeo, R., 2009. Studio geofisico integrato ad alta risoluzione dei depositi marini e della struttura del substrato della Riviera di Miramare (Golfo di Trieste). PhD Thesis. University of Trieste, p. 197.

Ronchi, L., Fontana, A., Novak, A., Correggiari, A., Poglajen, S., 2023. Late-Quaternary evolution of the semi-confined alluvial megafan of Isonzo River (northern Adriatic): where the fluvial system of the southern Alps meets the Karst. Geosciences 13, 135. https://doi.org/10.3390/geosciences13050135.

Rossi, V., Barbieri, G., Vaiani, S.C., Amorosi, A., 2021. Benthic foraminifers from Holocene subaqueous deltas of the Western Mediterranean: stratigraphic implications and palaeoenvironmental significance of the biofacies. Mar. Geol. 442, 106632.

Schattner, U., Lazar, M., Tibor, G., Ben-Avraham, Z., Makovsky, Y., 2010. Filling up the shelf - a sedimentary response to the last post-glacial sea rise. Mar. Geol. 278, 165–176.

Sgarrella, F., Moncharmont Zei, M., 1993. Benthic foraminifera of the gulf of Naples (Italy): systematics and autoecology. Bollettino Società Paleontologica Italiana 32, 145–264.

Siddall, M., Rohling, E.J., Almogi-Labin, A., Hemleben, Ch, Meischner, D., Schmelzer, I., Smeed, D.A., 2003. Sea-level fluctuations during the last glacial cycle. Nature 423, 853–858.

Shanley, K.W., McCabe, P.J., 1994. Perspectives on the sequence stratigraphy of continental strata. AAPG Bulletin 78, 544–568.

Soler, F., Moreno, D., Araujo, R., Ramos, M.A., 2006. Diversidad y distribuciónde los moluscos de agua dulce en la comunidad de Madrid (España). Graellsia 62, 201–252.

Soulié-Märsche, I., 2002. Les Charophytes comme biomarqueurs pour la reconstitution des paléoenvironnements lacustres. In: Miskovsky, J.C.L. (Ed.), book: Géologie de la Préhistoire. 2nd edition, Publisher: GEOPRE, Paris.

Stoker, M.S., Akhurst, M.C., Howe, J.A., Stow, D.A.V., 1998. Sediment drifts and contourites on the continental margin off northwest Britain. Sediment. Geol. 115, 33–51.

Swift, D.J.P., 1968. Coastal erosion and transgressive stratigraphy. J. Geol. 76, 444–456.

Tosi, L., 1994. L'evoluzione paleoambientale tardo-quaternaria del litorale veneziano nelle attuali conoscenze. Il Quat. 7, 589–596.

Trincardi, F., Correggiari, A., 2000. Quaternary forced regression deposits in the Adriatic basin and the record of composite sea-level cycles. In: Hunt, D., Gawthorpe, R.L. (Eds.), Sedimentary Responses to Forced Regressions, vol. 172. Geological Society Special Publication, pp. 245–269.

Trincardi, F., Argnani, A., Correggiari, A., 2011. Carta geologica dei mari italiani alla scala 1:250.000 - Foglio NL33-7 Venezia. Servizio Geologico d'Italia.

Trobec, A., Busetti, M., Zgur, F., Baradello, L., Babich, A., Cova, A., Gordini, E., Romeo, R., Tomini, I., Poglajen, S., Diviacco, P., Vrabec, M., 2018. Thickness of marine Holocene sediment in the gulf of Trieste (northern Adriatic Sea). Earth Syst. Sci. Data 10 (2), 1077–1092.

Zampa, L.S., 2014. Evidenze di subsidenza tettonica nel sistema di scarpata e terrazzi tardo-pleistocenici nel Golfo Di Trieste". Bachelor Thesis, University of Trieste, p. 63.

Zazo, C., Goy, J.L., Dabrio, C.J., Bardaj, T., Hillaire-Marcel, C., Ghaleb, B., González-Delgado, J.-A., Soler, V., 2003. Pleistocene raised marine terraces of the Spanish Mediterranean and Atlantic coasts: records of coastal uplift, sea-level highstands and climate changes. Mar. Geol. 194, 103–133.

Zecchin, M., Baradello, L., Brancolini, G., Donda, F., Rizzetto, F., Tosi, L., 2008. Sequence stratigraphy based on high-resolution seismic profiles in the late Pleistocene and Holocene deposits of the Venice area. Mar. Geol. 253, 185–198.

Zecchin, M., Brancolini, G., Tosi, L., Rizzetto, F., Caffau, M., Baradello, L., 2009. Anatomy of the Holocene succession of the southern Venice Lagoon revealed by very high-resolution seismic data. Continent. Shelf Res. 29, 1343–1359.

Zecchin, M., Caffau, M., Civile, D., Roda, C., 2010. Anatomy of a late Pleistocene clinoformal sedimentary body (Le Castella, Calabria, southern Italy): a case of prograding spit system? Sediment. Geol. 223, 291–309.

Zecchin, M., Ceramicola, S., Gordini, E., Deponte, M., Critelli, S., 2011. Cliff overstep model and variability in the geometry of transgressive erosional surfaces in high-gradient shelves: the case of the Ionian Calabrian margin (southern Italy). Mar. Geol. 281, 43–58.

Zecchin, M., Tosi, L., 2014. Multi-sourced depositional sequences in the Neogene to Quaternary succession of the Venice area (northern Italy). Mar. Petrol. Geol. 56, 1–15.

Zecchin, M., Ceramicola, S., Lodolo, E., Casalbore, D., Chiocci, F.L., 2015. Episodic, rapid sea-level rises on the central Mediterranean shelves after the Last Glacial Maximum: a review. Mar. Geol. 369, 212–223.

Zecchin, M., Caffau, M., Ceramicola, S., 2016. Interplay between regional uplift and glacio-eustasy in the Crotone Basin (Calabria, southern Italy) since 0.45 Ma: a review. Global Planet. Change 143, 196–213.

Zecchin, M., Donda, F., Forlin, E., 2017. Genesis of the northern Adriatic sea (northern Italy) since early Pliocene. Mar. Petrol. Geol. 79, 108–130.

Zecchin, M., Catuneanu, O., Caffau, M., 2019. Wave-ravinement surfaces: classification and key characteristics. Earth Sci. Rev. 188, 210–239.

Zecchin, M., Busetti, M., Donda, F., Dal Cin, M., Zgur, F., Brancatelli, G., 2022. Plio-Quaternary sequences and tectonic events in the northern Adriatic Sea (northern Italy). Mar. Petrol. Geol. 142, 105745.

Žvab Rožič, P., Vidović, J., Ćosović, V., Hlebec, A., Rožič, B., Dolenec, M., 2022. A multiparametric approach to unravelling the geoenvironmental conditions in sediments of Bay of Koper (NE AdriaticSea): indicators of benthic foraminifera and geochemistry. Front. Mar. Sci. 9, 812622 https://doi.org/10.3389/fmars.2022.812622.